(a) TITLE

AGO2 promotes telomerase activity and interaction between the telomerase components TERT and TERC

(b) authors' full names

Ilaria Laudadio[1*], Francesca Orso[2], Gianluca Azzalin[1], Carlo Calabrò[1], Francesco Berardinelli[3], Elisa Coluzzi[3], Silvia Gioiosa[4], Daniela Taverna[2], Antonella Sgura[3], Claudia Carissimi[1+] and Valerio Fulci[1+]

(c) affiliations

[1]Dept. of Cellular Biotechnology and Hematology, "Sapienza" University of Rome, Italy;

[2]Molecular Biotechnology Center, Dept. Molecular Biotechnology and Health Sciences, University of Turin, Italy

[3] Dept of Science, University of Rome "Roma Tre", Italy

[4] Istituto di Biomembrane, Bioenergetica e Biotecnologie Molecolari (IBIOM), CNR, Bari, Italy

[*] corresponding author: Ilaria Laudadio ilaria.laudadio@uniroma1.it

[+] co-last authors

(d) running head

AGO and sRNA control telomerase activity

(e) keywords

Non-coding RNA, Argonaute, Telomerase, Telomere, Cancer

ABSTRACT

Telomerase reverse transcriptase (TERT) and telomerase RNA component (TERC) constitute the core telomerase enzyme that maintains the length of telomeres. Telomere maintenance is affected in a broad range of cancer and degenerative disorders. Taking advantage of gain and loss-of-function approaches, we show that ARGONAUTE2 (AGO2) controls telomerase activity and stimulates the association between TERT and TERC. AGO2 depletion results in shorter telomeres as well as in lower proliferation rate *in vitro* and *in vivo*. We also demonstrate that AGO2 interacts with TERC and with a newly identified sRNA (*terc*-sRNA), arising from the H/ACA box of TERC. Notably, *terc*-sRNA is sufficient to enhance telomerase activity when overexpressed. Analysis of sRNA-Seq datasets shows that *terc*-sRNA is detected in primary human tissues and increases in tumors as compared to control tissues. Collectively, these data uncover a completely new layer of complexity in the regulation of telomerase activity by AGO2 and might lay the foundation for the exploitation of new therapeutic targets for tumors and telomere diseases.

INTRODUCTION

Telomeres, the specialized nucleoprotein complexes present at the ends of linear eukaryotic chromosomes, play essential roles in maintaining genome stability and controlling cell proliferation. The length of human telomeric DNA is maintained by the addition of TTAGGG repeats to telomeres by a ribonucleoprotein (RNP) enzyme, telomerase. The catalytic components of the telomerase RNP are the telomerase reverse transcriptase (TERT) and the H/ACA box telomerase RNA (TERC), which is the template used for the synthesis of telomeres. TERT and TERC are necessary and sufficient for this reaction [1]. However *in vivo*, the telomerase holoenzyme also includes the accessory proteins dyskerin (DKC1), NOP10, NHP2 and GAR1 [2]. The formation of the catalytically active telomerase holoenzyme is a highly elaborate and multistep process of RNA maturation, assembly and trafficking within the nucleus [3].

Most human somatic cells express insufficient or undetectable levels of telomerase; thus, telomeres shorten at each cell division, reaching a critical threshold, which triggers cellular senescence. On the contrary, continuously dividing cells such as germ cells, stem cells, and expanding lymphocytes require telomerase activity for maintaining telomere length and surviving. Deficiencies in telomerase activity, maturation, or recruitment to telomeres can lead to human telomeropathies, such as aplastic anemia and dyskeratosis congenita [4]. On the other hand, telomerase activity is highly elevated in 85%–90% of human cancers and in over 70% of immortalized human cell lines [5][6], suggesting that the activation of telomerase is crucial for continued cell proliferation. Hence, greater knowledge of telomerase biology and regulation is required to increase our understanding of both human diseases and natural cellular processes.

Argonaute (AGO) proteins are small RNA (sRNA)-binding proteins which use the sequence information encoded in the sRNA as a guide to identify complementary target RNAs. Humans have four AGO proteins, AGO1, AGO2, AGO3 and AGO4, sharing about 80% identity in their amino acid sequences [7]. Among them, only AGO2 has retained the ability to cleave target RNAs [8]. The most studied function of AGO proteins is post-transcriptional gene silencing in association with

microRNAs. However in the last years, sRNA profiling by next-generation sequencing (sRNA-Seq) allowed the identification of novel classes of sRNAs bound to AGO proteins in mammalian cells, in addition to miRNAs [9] [10] [11] [12]. Moreover, recent evidences involve AGO proteins in nuclear processes such as transcriptional gene silencing [13][14], DNA damage [15], chromatin remodeling [9] and splicing [16][17]. These new data strongly suggest that AGO proteins can exert previously unexpected functions.

Here, we identify a new function of AGO2 in human telomerase biology. Modulation of AGO2 expression by loss- and gain-of-function approaches results in changes in telomerase activity. Taking advantage of an AGO2 knock-out (KO) human cell line, we demonstrate that AGO2 controls the association between TERT and TERC and this results in telomere shortening, lower proliferation rate *in vitro* and tumor growth *in vivo*. We further discover a new AGO2-bound sRNA, herein referred to as *terc*-sRNA, which arises from the H/ACA domain of TERC. *Terc*-sRNA is detected not only in human cell lines but also in primary human tissue and its expression increases in tumor samples as compared to non-tumor tissues. Interestingly, overexpression of *terc*-sRNA is sufficient to increase telomerase activity. Together, these data show that AGO2 and the newly identified *terc*-sRNA are novel players in human telomerase regulation.

RESULTS

Proliferation and tumor growth are affected by AGO2 depletion.

AGO2 encodes for the only member of the AGO protein family that retains endonucleolytic activity in human cells [8]. While the roles of AGO2 in miRNA mediated post-transcriptional regulation and RNAi have been thoroughly characterized, the roles of AGO2 in the nucleus of human cells, including a role in DNA damage [15], chromatin remodeling [9] and splicing [16], are currently beginning to be elucidated. Because of these unexpected functions of human AGO2, an experimental tool to evaluate AGO2 novel functions in human cell biology is required. Therefore, we took advantage of genome editing to generate inactivating mutations in all three copies of the *AGO2* locus present in

the human cell line HeLaS3 by using Zinc Finger Nucleases (AGO2KO cells) [18].

Firstly, we investigated how AGO2 depletion might influence cell proliferation and survival. Comparison of growth curves of parental and AGO2KO HeLaS3 cells highlighted that the absence of AGO2 impaired the proliferative capacity of HeLaS3 cells (Fig 1A). Similarly, the results of colony formation assay also showed that clonogenic survival was decreased in AGO2KO cells as compared to HeLaS3 (Fig 1B). We also assessed *in vivo* proliferation of AGO2KO cells by injecting subcutaneously immunocompromised mice with parental HeLaS3 and AGO2KO cells. In line with *in vitro* assays, when we measured tumors diameter at different time points (Fig 1C) and tumor weight at 30 days post-injection (Fig 1D), we found that AGO2 depletion inhibits the growth of HeLaS3 xenografts in nude mice.

Next, we profiled the transcriptome of HeLaS3 and AGO2KO cells by microarray. Microarray analysis showed that only 12 genes are differentially expressed in AGO2KO compared to wild-type cells (FDR < 0.01) (Appendix figure S1). Since the endpoint of the microRNA pathway is mRNA degradation, these data suggest that AGO2 is unlikely to control proliferation in human cells via miRNA-mediated regulation of gene expression [19], suggesting the existence of an alternative mechanism.

AGO2 interacts with a sRNA arising from TERC locus (*terc*-sRNA)

Several recent papers show that AGO proteins interact with small RNAs other than miRNAs, displaying novel roles in particular in the nuclear compartment [15][16][17][14][9]. We recently published that in the nuclei of human cells AGO2 is bound to sRNAs arising from transcriptional termination sites (TTSa-RNAs). We found that AGO2-bound TTSa-RNAs derive from genes involved in cell cycle progression regulation [18]. In HeLaS3 and HCT116 cell lines nuclear AGO2 interacts with a 23 nt-sRNA arising from TTS of the telomerase RNA component TERC (positions 425 to 447), herein referred to as *terc*-sRNA (Fig 2A). Based on its association with AGO2, its specific size and the fact that almost no reads map on TERC RNA outside positions 425 – 447 (Fig EV 1A), we conclude that *terc*-sRNA is not a mere by-product of TERC degradation, but it is a

specific, biologically-generated sRNA. We further confirmed that TERC is the precursor of *terc*-sRNA by stably overexpressing TERC in HeLaS3 cells by lentiviral transduction (Fig 2B). Indeed, we found higher levels of *terc*-sRNA in sRNA fraction (< 100nt) of TERC-overexpressing cells than in control cells (Fig 2C), as assessed by RT-qPCR using specific primers [20] (Appendix Figure 2A-C).

In human cells, impairment of core components of telomerase RNP, TERC and TERT, not only determines short telomeres, but also affects proliferation and colony forming efficiency, mimicking the phenotype we observed in AGO2KO cells [21][22]. As a consequence, we hypothesized that AGO2 and *terc*-sRNA might be involved in telomerase-mediated telomere lengthening.

AGO2 controls telomere lengthening and enhances telomerase activity.

To verify this hypothesis, we compared relative telomere length in parental and AGO2KO HeLaS3 by quantitative PCR [23]. The ratio of the copy number of telomeric repeats (T) and the copy number of a reference gene was calculated. As a reference, we used multicopy genes, with thousands of copies throughout the genome, similar to telomeres (*Alu* in Fig 3A and *18S* in Appendix figure S3A), as well as *36B4* (Appendix figure S3A), which is a four-copy gene in HeLaS3 cells. Regardless to the reference we used, average telomere length in AGO2KO cells was 70% shorter than parental cells.

In order to further confirm the observed telomere shortening and analyze single telomere length distributions in AGO2KO and HeLaS3 cells, centromere-calibrated telomeric QFISH was performed (Fig 3B). Histograms of telomere length frequencies showed a proportion of short telomeres much higher in AGO2KO cells than in control cells (Fig 3C) and the difference in telomere length was extremely significant and affected both q and p arms (Fig 3C and Appendix figure S3B). In particular, comparing the percentage of telomeres shorter than 3 arbitrarily chosen thresholds (*i.e.* 5, 10 and 15 T/C%), we always found a very significantly higher proportion of eroded telomeres in AGO2KO cells than in HeLaS3 cells (Appendix figure S3C).

Notably, when we measured telomerase activity via Telomerase Repeated Amplification Protocol

(TRAP) [24], we observed a decreased telomerase activity in AGO2KO cells as compared to parental cells (Fig 3D, E). Coherently, this phenotype was partially rescued by stable overexpression of FLAG/HA-tagged AGO2 (FH AGO2) in AGO2KO cells (Fig 3F, Appendix figure S3D). To further confirm that AGO2 expression can modulate telomerase activity, we stably overexpressed FH AGO2 in HeLaS3 parental cells (HeLaS3_FH AGO2; Appendix figure S3E) and we performed analysis of telomerase activity (Fig 3 G). In line with the results obtained in AGO2KO cells, overexpression of AGO2 was sufficient to enhance telomerase activity as compared to control cells. These data show that AGO2 controls telomere elongation capacity and telomerase activity in human cells, pointing out AGO2 as a new player in telomere lengthening.

AGO2 affects the association between TERT and TERC

We next focused our attention on the mechanism by which AGO2 controls telomerase activity. We hypothesized that AGO2 might directly or indirectly control expression levels of TERT and /or TERC. However, neither TERC RNA levels (Fig 4A), nor TERT protein levels (Fig 4D, E) were affected by AGO2 depletion.

Furthermore, it has been reported that 3'-extended or polyadenylated isoforms of TERC are post-transcriptionally processed in order to give rise to mature non-polyadenylated 451 nt-long TERC and that this processing is required for telomere maintenance [25][26]. We therefore checked if AGO2 regulates telomerase activity by controlling TERC maturation. We quantified 3'-extended and oligo-adenylated TERC by random hexamer- and oligo d(T)-primed qRT-PCR respectively, but we did not detect any change in the abundance of immature forms of TERC when AGO2 is ablated (Fig 4B, C). Finally, we aimed to study if the assembly of the core components of telomerase RNPs, namely TERC and TERT, was affected in AGO2KO cells. By RIP, we looked at endogenous TERC-TERT interaction in both parental and AGO2KO HeLaS3 cells. Notably, we found that enrichment of TERC in TERT-IPed RNA is impaired in AGO2KO cells, as compared to parental HeLaS3 (Fig 4F). As a negative control, we analyzed HOTAIR, which is not enriched in TERT-IP as compared to mock IP

(IgG). No variation in HOTAIR enrichment in TERT-IP samples can be detected between AGO2KO and parental HeLaS3. Coherently, re-expression of AGO2 in AGO2KO cells (AGO2KO_FH AGO2) increased association between TERT and TERC as compared to AGO2KO control cells (AGO2KO_GFP; Fig 4G). Importantly no protein-protein interaction between AGO2 and TERT could be detected by co-immunoprecipitation assay (Fig 4H), suggesting that AGO2 is not part of telomerase RNPs.

Overall, our data indicate that AGO2 regulates telomerase activity through the control of TERT association with TERC in the assembly of active telomerase RNP.

AGO2 is recruited on TERC.

Since AGO2 is an RNA binding protein we checked for interaction between AGO2 and TERC RNA. We firstly performed RIP with an antibody against AGO2 from HeLaS3 cells and we found an enrichment of TERC RNA in AGO2-IP as compared to IgG, as assessed by RT-qPCR (Fig 5A). Association between AGO2 and TERC was further verified by immunoprecipitating FH AGO2 from HeLaS3_FH AGO2 and HeLaS3_GFP cells (as a negative control) with an HA antibody (Fig 5B).

We additionally demonstrated the interaction between AGO2 and TERC by taking advantage of HeLaS3 cells stably overexpressing TERC (Fig 2B). Ectopically expressed TERC RNA (ectoTERC) can be discriminated by RTqPCR from the endogenously expressed one, because it is transcribed from the integrated lentiviral vector as a longer RNA tagged with a specific sequence downstream the 3'end of TERC coding region. Indeed, using specific primers, ectoTERC RNA was detected only in HeLaS3_TERC but not in control HeLaS3 cells (HeLaS3_GFP) (Appendix figure S4A). We immunoprecipitated AGO2 and we found that it is also bound to the ectopically expressed TERC RNA (Appendix figure S4B).

Through base pairing, AGO2-loaded sRNAs recognize complementary RNAs as their targets. *Terc*-sRNA arises from the right arm of the terminal hairpin of TERC, displaying a good complementarity to the left arm of this hairpin. Therefore, we looked for putative target sites of *terc*-sRNA in TERC

RNA by using the RNA-hybrid program, which finds the energetically most favorable hybridization sites of a sRNA in a large RNA [27]. Surprisingly, the two-best pairing between TERC and *terc*-sRNA involved positions 313-340 of TERC, in the conserved region 4 (CR4)/CR5 domain of TERC (minimum free energy: -30 Kcal/mol) and positions 12-31 of TERC, localized in the template boundary element (TBE) at the 5'end of TERC (minimum free energy: -29.4 Kcal/mol) (Appendix figure S4C-D).

These data suggest that *terc*-sRNA not only originates from TERC RNA, but might also target TERC RNA in two different binding sites, guiding interaction between AGO2 and TERC by base pairing.

Finally, in order to verify whether the interaction between AGO2 and TERC is mediated by *terc*-sRNA predicted sites, we destroyed complementarity by mutating TERC sequence in positions 313-340 and by deleting TERC positions 12-31 in the lentiviral vector coding for ectoTERC (TERC(313-340mut) and TERC (Δ 12-31), respectively). HeLaS3 cell were transduced with mutated TERC-coding lentiviral particles (HeLaS3_TERC(313-340mut) and HeLaS3_TERC (Δ 12-31)). The expression levels of ectoTERC were comparable in HeLaS3_TERCwt, HeLaS3_TERC(313-340mut) and HeLaS3_TERC (Δ 12-31) (Appendix figure S4E). We next checked association between AGO2 and ectoTERC, by immunoprecipitating AGO2-associated RNA from lysates of cells expressing the different TERC variants. As shown in Fig 5C, when we compared ectoTERC-AGO2 binding in HeLaS3_TERCwt, HeLaS3_TERC(313-340mut) and HeLaS3_TERC (Δ 12-31), we found that enrichment of ectoTERC in RIP AGO2 samples decreases when *terc*-sRNA binding sites are mutated. Overall, these data demonstrate that AGO2 binds to TERC. Moreover, positions 313-340 and 12-31 of TERC, displaying base-complementarity with *terc*-sRNA, are required for this interaction, strongly suggesting that *terc*-sRNA guides AGO2 onto TERC.

Terc-sRNA biogenesis does not involve DICER or AGO2.

By sRNA-Seq, we showed that AGO2 binds to *terc*-sRNA (Fig EV1A). To confirm this interaction, we immunoprecipitated endogenous AGO2 in HeLaS3 whole-cell extract and we amplified *terc*-

sRNA by qRT-PCR (Fig EV1B-C). In line with high-throughput data, *terc*-sRNA is enriched in AGO2-IP sample as compared to mock IP, performed using matched immunoglobulin.

Terc-sRNA derives from a stem-loop structure (Fig 2A), reminiscent of miRNA precursors. We hypothesized that DICER or AGO2, both of which are known to control miRNA processing and stability [28], could be involved in *terc*-sRNA biogenesis. To answer this question, we compared *terc*-sRNA abundance by RT-qPCR in the sRNA fraction isolated from HCT116 and HCT116 Dicer^{EX5} (a subclone of HCT116 cells in which DICER has been impaired) [29] and from parental and AGO2KO HeLaS3 cell lines (Appendix figure S2D-E, Fig EV1D-F). Impairment of DICER or AGO2 catalytic activity did not determine any changes in *terc*-sRNA levels. On the contrary, miRNA expression is downregulated in HCT116 Dicer^{EX5} and AGO2KO HeLaS3 cells as compared to matched wild-type cells (Fig EV1E and G). We concluded that *terc*-sRNA can be processed independently of DICER and AGO2. In agreement with these observations, we could not find any evidence for a small RNA duplex as a precursor of *terc*-sRNA processing. Indeed, neither reads arising from the complementary 5' strand of the stem-loop structure nor reads arising from antisense transcription can be detected (Appendix figure S5).

Terc-sRNA overexpression increases telomerase activity.

We next investigated whether modulation of *terc*-sRNA levels can control human telomerase activity. We overexpressed *terc*-sRNA in parental HeLaS3 cells through transient transfection of a synthetic *terc*-sRNA or a control siRNA (ctl-siRNA) and checked telomerase activity via TRAP assay. As shown in Fig 6A-B, *terc*-sRNA transfected HeLaS3 cells displayed higher telomerase activity as compared to ctl-siRNA transfected cells, mimicking the effect of AGO2 overexpression (Fig 3G) and suggesting that the role of AGO2 in telomere biology might be, at least in part, mediated by *terc*-sRNA.

Furthermore, in order to study if stimulation of telomerase activity by *terc*-sRNA requires AGO2, we overexpressed synthetic *terc*-sRNA or ctl-siRNA in AGO2KO cells (Fig 6A-B). Surprisingly, in

AGO2KO cells *terc*-sRNA overexpression was sufficient to recover telomerase activity deficit caused by AGO2 depletion. These data unravel that abundance of *terc*-sRNA modulates telomerase activity in human cells, and that activity of *terc*-sRNA is not strictly dependent upon AGO2 expression.

Therefore, we postulated that not only AGO2 but also other AGO proteins might bind *terc*-sRNA, and TERC and participate in telomerase biology. Indeed, AGO members are mainly considered to be functionally redundant as far as loading of sRNAs, such as miRNAs, is concerned [30][31][32]. We focused our attention on AGO1, which is the second most abundant AGO protein in HeLaS3, behind AGO2 [33]. We reanalyzed data of sRNA-seq that we previously obtained from immunoprecipitation of AGO1 from nuclei of HeLaS3 [9], looking for sRNAs mapping on *TERC* locus. AGO1 binds a sRNA deriving from TERC 3'end and corresponding to *terc*-sRNA (Fig EV2A). We validated this interaction by immunoprecipitating endogenous AGO1 from HeLaS3 whole-cell extract, and by RT-qPCR we demonstrated that both *terc*-sRNA and TERC are enriched in AGO1-IP RNA as compared to mock IP-RNA (IgG) (Fig EV2B-D). This evidence suggests that also AGO1 might be involved in the control of telomerase activity. To answer this question, we genetically inactivated *AGO1* loci in both parental HeLaS3 and AGO2KO cells by CRISPR/Cas9. We generated two independent AGO1KO and two AGO1/AGO2 double KO (AGO1/AGO2dKO) monoclonal cell lines (Appendix figure S6A). As controls, we isolated subclones from parental HeLaS3 and AGO2KO cells following transduction with CRISPR/Cas9 control vector (HeLaS3 WT CRISPR neg and AGO2KO CRISPR neg). We analyzed telomerase activity by TRAP and we could not detect any difference between AGO1KO and HeLaS3 WT CRISPR neg cells. Moreover, telomerase activity of AGO1/AGO2dKO cells is comparable to what observed in AGO2KO CRISPR neg cells (Fig EV2E, Appendix figure S6B). In conclusion, AGO1 depletion does not impact telomerase activity neither in wild type nor in AGO2KO background, suggesting that AGO2 is the major player of this new mechanism. Otherwise under extreme conditions, such as overexpression of *terc*-sRNA, also AGO1 might mediate the activity of this sRNA.

Terc-sRNA is detected in primary human samples and is overexpressed in tumor tissues

Finally, we asked if *terc*-sRNA can be detected in primary human tissues. We looked for publicly available datasets in which microRNA profile was assessed by NGS, and we identified five datasets containing sRNA expression profiles in tumor samples and control tissues (normal, adjacent or benign tumors). In all datasets analyzed, we could detect *terc*-sRNA expression (Fig EV3A) in both tumor samples and control tissues, thus confirming that this small RNA is expressed in primary human tissues.

Moreover, given that de-regulation of other sRNA classes has been reported in human tumors [34][35], and that *in vitro* overexpression of *terc*-sRNA increases telomerase activity, thus possibly conferring a selective advantage to cells over-expressing this sRNA (Fig 6), we also compared *terc*-sRNA abundance in tumor samples and control tissues. Interestingly, we highlighted that *terc*-sRNA is significantly overexpressed in breast cancer and in lung adenocarcinoma as compared to normal tissues. In adrenocortical tumors, we found a significant increase of *terc*-sRNA in carcinoma as compared to adenoma. The lack of statistical significance of the result obtained in endometrial cancer dataset is likely due to the small number of samples in this dataset (n=6) (Fig EV3B). Notably, due to lack of matched long non-coding RNA expression data, we could not quantify TERC expression in the same samples, hence we cannot rule out the possibility that *terc*-sRNA overexpression in tumor samples is due to TERC over-expression in the same samples.

DISCUSSION

Telomerase activity is undetectable in most human somatic cells. Thus, telomere length decreases across each cycle of cell division and when telomeres reach a critically short length, cell senescence is induced. However, certain human cell populations such as germ cells, stem cells, and expanding lymphocytes, express telomerase, and thereby, maintain telomere length and escape from cellular

senescence. Defects in genes involved in telomerase biology affect the renewal of critical stem cell populations, particularly in highly proliferative tissues, and cause a spectrum of disorders referred to as telomeropathies [36]. On the other hand, improper activation of telomerase in somatic cells contributes to tumorigenesis because it enables neoplastic cells to proliferate indefinitely. Indeed, reactivation of TERT expression is a hallmark of carcinogenesis and is seen in more than 80%–90% of tumors [37]. Thus, deeper characterization of telomerase regulation is attractive for the development of novel therapeutic targets and biomarkers in a wide range of pathologies.

Here, we describe a new and unanticipated role for AGO2 in controlling human telomerase activity through the regulation of association between the telomerase core components, TERT and TERC. Furthermore, we identified *terc*-sRNA as a novel AGO-associated sRNA arising from the right arm of the terminal hairpin of the H/ACA box of TERC and whose over-expression promotes telomerase activity in human cells.

In mammalian cells, there are 4 AGO proteins (AGO1–4) which are key components of miRNA-mediated post-transcriptional modulation of gene expression. We show that depletion of AGO2 by genome editing in the human cell line HeLaS3 determines impaired proliferation and colony forming efficiency as well as telomere shortening and decreased telomerase activity, a phenotype reminiscent of those caused by telomerase core components (TERC and TERT) decrease. These effects of AGO2 ablation might be the results of an impairment in miRNA function. Indeed, the absence of AGO2 could deregulate the expression of genes involved in telomerase biology. However, when we profiled transcriptome of HeLaS3 and AGO2KO cells by microarray, only 12 genes were deregulated in AGO2KO cells (FDR< 0.01), suggesting that AGO1/3/4 might mostly compensate lack of AGO2 as far as loading of miRNA is concerned [38][31]. Importantly among differentially expressed genes, no gene directly involved in telomerase biology can be found. Coherently, TERC RNA and TERT protein levels are not affected by AGO2 depletion. These data suggest that AGO2 is unlikely to control telomere lengthening via deregulation of gene expression, but probably through alternative mechanisms.

Interestingly we showed that AGO2 as novel TERC-binding protein. While impairment of previously described TERC binding proteins, such as DKC1 [39], NOP10 [40], NHP2 [41], NAF1[42] and FXR1 [43], cause defects in telomere maintenance by affecting TERC stability, we show that AGO-TERC interaction is unlikely to control TERC abundance. Moreover, this interaction is impaired by mutations of TERC sequence in positions 313-340 in CR4/CR5 domain. Interestingly, in human cells depletion of TERC residues 225-348 [44] and a mutation of TERC (G319A) [45] do not alter TERC overall levels but compromise telomerase function by decreasing binding of TERC to TERT *in vitro* and *in vivo*. Since AGO2 depletion affects the association between TERC and TERT, we speculate that AGO-TERC interaction might stimulate assembly of active telomerase RNPs. An intriguing possibility is that binding of AGO to TERC might drive TERC folding. This hypothesis would recapitulate what previously described in ciliate telomerase biogenesis. In *Tetrahymena thermophile*, interaction between the stem terminus element of telomerase RNA (corresponding to CR4/CR5 domain in vertebrates) and a La-motif RNA binding protein induces structural rearrangement of telomerase RNA, which in turn promotes the binding of TERT to form the functional telomerase complex [46]. Interestingly, reconstitution in *vitro* of human telomerase is highly dependent on the folding state of TERC, suggesting that TERC folding is a limiting factor in vertebrate telomerase assembly as well [47][48].

Terc-sRNA is predicted to target sequences in CR4/CR5 (positions 313-340) and in the TBE domains (positions 12-31) of TERC. The integrity of these predicted binding sites on TERC is required for AGO2 binding to TERC, strongly suggesting that *terc*-sRNA drives AGO2 onto its target TERC via base-complementarity. Moreover, *terc*-sRNA overexpression results in higher telomerase activity, mimicking the effect of AGO2 overexpression. A possible explanation for this data is that *terc*-sRNA recognizes TERC and recruits AGO2 and additional still-unknown factors to TERC RNA, driving AGO2 effects on TERC-TERT association. Although our experimental observations demonstrate a role for *terc*-sRNA in telomerase biology, a conclusive evidence that AGO2/*terc*-sRNA/TERC complexes mediate AGO2-dependent stimulation of telomerase activity is still lacking. Indeed, since

terc-sRNA and TERC share the same sequence and arise from the same locus, any *terc*-sRNA loo-of-function approach either via antisense oligonucleotides or genome-editing will target both *terc*-sRNA and TERC, making any interpretation of this manipulation misleading. Therefore, further efforts are required to disclose if AGO/*terc*-sRNA complexes are required to control telomerase activity and to explore the hypothesis that other still-unidentified sRNAs (miRNAs or others) could cooperate with AGO2 in this process.

Notably, we show that *terc*-sRNA is expressed in primary human tissues. Furthermore, *terc*-sRNA is overexpressed in different cancers. Several expression studies have found that also AGO2 is highly expressed in different kinds of tumors such as breast cancer, high-risk myeloma, colon cancer, liver cancer, and gastric carcinoma[49]. Since our results demonstrate that AGO2 and *terc*-sRNA are able to modulate telomerase activity in human cell lines, we speculate that concomitantly reactivation of TERT expression and overexpression of AGO2 and/or *terc*-sRNA might confer a selective advantage to tumor cells and probably a more aggressive phenotype. However, lack of information on TERC expression in the datasets we analyzed does not allow us to assess whether the observed *terc*-sRNA over-expression is a consequence of TERC over-expression. Therefore, we believe that further investigation will be required to unravel the relationship between TERC and *terc*-sRNA in primary human tissues as well as to validate of *terc*-sRNA and AGO proteins as valid biomarkers for diagnosis or prognosis of human malignancies.

Finally, it was shown that several mutations correlated to dyskeratosis congenita reduce but do not abolish TERC expression ([50] [51] [25] [40] [41]). Therefore, modulation of AGO or *terc*-sRNA levels might enhance the interaction between TERT and residual TERC and partially counteract telomere shortening in patients affected by this degenerative disorder.

Overall, insights from this work might be the starting point for future investigation of AGO proteins and *terc*-sRNA as biomarkers and/or therapeutic targets to modulate telomerase activity and self-renewal in tumors and telomeropathies.

MATERIALS AND METHODS

Cell culture and transfection

Parental and AGO2KO [18] HeLaS3 cells were grown in DMEM medium supplemented with 10% (v/v) fetal bovine serum, 2mM L-Glutamine and Penicillin-Streptomycin. HCT116 and HCT116 $DICER^{Ex5}$ cells [29] were grown in McCoy's 5A medium supplemented with 10% (v/v) fetal bovine serum, 2mM L-Glutamine and Penicillin-Streptomycin. AGO1KO and AGO1/AGO2dKO monoclonal cell lines were obtained by using CRISPR/Cas9 technology. HeLaS3 and AGO2KO cells were transduced with a lentiviral vector (LentiAGO1CRISPR v2, GeneScript) coding for a gRNA sequence targeting AGO1 (TCAGCGCGTTCGCTTCACCA) or an empty vector (LentiCRISPR v2, a gift from Feng Zhang, Addgene plasmid # 52961 [52]) as a control. Transduced cells were selected by puromycin for 2 days. Individual clones were isolated by serial dilution and assayed by Western Blot for AGO1 expression. KO of all *AGO1* alleles was confirmed by Sanger sequencing. Overexpression of terc-sRNA was performed by transfecting 20 nM siRNAs (*terc*-sRNA: UGCACCCAGGACUCGGCUCACA(Sigma);ctl-siRNA: GCUUCAUAAGGCGCAUGC[dT][dT]) for 4 days using INTERFERin®, according to the manufacturer's instructions (Polyplus Transfection).

Cell proliferation assays

For cell proliferation curves, $8x10^4$ cells were seeded in 12-well plate. Cells were counted every 24h for 5 days using EVE™ Automated Cell Counter, (NanoEnTek). For the colony-formation assay, 500 cells were placed into each well of a six-well plate and maintained in media containing 10% FBS for 11 days, replacing the medium every 4 days. Colonies were fixed and stained with crystal violet (0.5%w/v) in 20% methanol for 30min, plate was washed in PBS, and counted using a microscope.

In vivo tumor growth

All experiments performed with live animals complied with ethical care. 5×10^6 parental or AGO2KO HeLaS3 cells (in PBS) were subcutaneously injected into the flanks of 8- to 12-week-old

NOD/SCID/IL2R_null (NSG) immunocompromised mice and tumor diameters were measured twice a week. Tumors were harvested 30 days following injection and weighted.

Q-PCR Assay for Average Telomere Measurement

Genomic DNA was isolated from 1x 10^6 cells using GenElute™ Mammalian Genomic DNA Miniprep (Sigma), according to manufacturer's protocol. Average telomere length was measured from total genomic DNA by using the qPCR method previously described [53]. Briefly, Q-PCR was performed using 35 ng of genomic DNA, 0.25µM of reverse and forward primers and GoTaq® qPCR Master Mix (Promega). Primers for telomeric repeats (T) and *36B4*, *Alu*, *18S* references (R) were as published in [54]. The relative average telomere length was termed the T/R ratio calculated using the $2^{-\Delta\Delta Ct}$ method.

Centromere-calibrated Quantitative FISH (Q-FISH)

Centromere-calibrated Q-FISH staining was performed as described previously [55] with minor modifications. Briefly, 48 h after seeding, slides were rinsed with phosphate-buffered saline (PBS), pH 7.5, and fixed in 4% formaldehyde for 2 min. After two rinses in PBS, the slides were incubated in acidified pepsin solution for 10 min, rinsed and dehydrated through graded alcohols. Slides and probes (Cy3 linked telomeric and chromosome 2 centromeric PNA probe, DAKO Cytomatation, Denmark) were co-denatured at 80°C for 3 min and hybridized for 2 h at room temperature in a humidified chamber. After hybridization, slides were washed twice for 15 min in 70% formamide, 10 mM Tris, pH 7.2, and 0.1% BSA followed by three 5-min washes in 0.1 M Tris, pH 7.5, 0.15MNaCl and 0.08%Tween 20. Slides were then dehydrated with an ethanol series and air dried. Finally, slides were counterstained with 4,6-diamidino-2 phenylindole (DAPI, Sigma Aldrich, St. Louis, MO) in Vectashield (Vector Laboratories, Burlingame, CA). Images were captured at 633 magnification with an Axio Imager M1 (Carl Zeiss, Germany) equipped with a CCD camera, and the telomere size was analyzed with ISIS software (MetaSystems, Germany). The software calculates telomere lengths as the ratio between the fluorescence of each telomere signal and the fluorescence

of the centromere of chromosome 2, used as the internal reference in each metaphase analyzed. Data were expressed as a percentage (T/C%) [56].

Telomerase Repeated Amplification Protocol (TRAP)

TRAP assay was performed as previously described [57] with minor changes. Briefly, $3x10^5$ cells were lysed on ice for 30 minutes in 300µl of NP-40 lysis buffer (10 mM Tris-HCl pH 8.0, 1 mM $MgCl_2$, 1 mM EDTA , 1% v/v NP-40, 0.25 mM Sodium deoxycholate, 10% v/v Glycerol, 150 mM NaCl, 5 mM 2-mercaptoethanol, protease inhibitor cocktail Sigma, RiboSafe RNase Inhibitor Bioline). Different serial dilutions of cellular lysates were added to TRAP mix, containing TRAP buffer 1x (20mM Tris-HCl pH 8.3, 1.5mM $MgCl_2$, 6.3mM KCl, 0.05% v/v Tween 20, 1mM EGTA), 0.2mM dNTPs, 4µG BSA, 100ng ACX primer, 100ng NT primer, 100 ng TS primer and 0.01 attomol of the internal control TSNT, in a final volume or 50µl. Ten µl of each sample was incubated at 85°C for 10 minutes to inactivate telomerase. Heat-inactivated samples were included in the TRAP assay as a negative control. Telomerase extension was next performed at 25°C for 40 minutes. PCR amplification of extension product was performed following addition of 1.25units of Taq DNA Polymerase (New England Biolabs) to TRAP samples. Products were resolved on 10% TBE polyacrylamide gels and visualized by staining with Ethidium Bromide using Chemidoc Imaging System (Biorad). Intensity of the telomerase products (6 bp-ladder) was determined by ImageLab Software (Biorad) and normalized with the intensity of the Internal Control (IC).

Plasmid and Lentiviral transduction

FLAG/HA AGO2 coding sequence was PCR-amplified from VP5- FLAG/HA AGO2 plasmid (a kind gift from Dr. G. Meister) with primers that introduce BamHI restriction sites at 5'end and SalI restriction site at 3'end of the sequence. TERC coding sequence was PCR-amplified from HeLaS3 genomic DNA with primers that introduce BamHI restriction sites at 5'end and SalI restriction site at 3'end of the sequence. PCR products were digested with BamHI and SalI and cloned in the lentiviral plasmid pLenti CMV GFP Puro (658-5) (a gift from Eric Campeau (Addgene plasmid # 17448) [58]), in order to replace GFP open reading frame and originate pLenti CMV FH AGO2 and pLenti CMV

TERC wt lentiviral plasmids. Viral particles were obtained by co-transfection of 293T-cells with lentiviral plasmids and the PLP-1, PLP-2 and PLP-VSVG plasmids (Invitrogen) and concentrated by ultra-centrifugation. HeLaS3 and/or AGO2KO cells were transduced and selected with puromycin.

TERC mutagenesis

Terc-sRNA binding site spanning positions 313-340 of TERC (GTCAGCCGCGGGTCTCTCGGG GGCG), was mutated in AGACTGGCCCGGCTGTCACCGCGCCC (mutated nucleotides are underlined), using Q5 Site-Directed Mutagenesis Kit (NEB) following manufacturer's protocol. Primers for mutagenesis were as follows: Fw TGTCACCGCGCCCAGGGCGAGGTTCAGGCCTT, Rev GCCGGGCCAGTCTGAGCCCAACTCTTCGCGGTG. *Terc*-sRNA binding site spanning positions 12-31 of TERC (GGTGGGCCTGGGAGGGGTGG) was deleted, using Q5 Site-Directed Mutagenesis Kit (NEB) following manufacturer's protocol. Primers for mutagenesis were as follows: Fw GGCCATTTTTTGTCTAACCCTAACTGAGAAGG, Rev CTCCGCAACCCGGTGGCG. Mutations were verified by Sanger sequencing.

RNA Immunoprecipitation (RIP)

For RNA immunoprecipitation from whole-cell extract, $60x10^6$ of cells were lysed in 3 ml of IP-buffer (150 mM KCl; 25 mM NaCl; 2 mM EDTA; 0.5% NP40; 0,05% Sodium deoxycholate; 0.5 mM DTT; protease inhibitor (Sigma); RiboSafe RNase Inhibitor (Bioline)) for 20 min on ice. Lysate was clarified by centrifugation at 16,000 g for 10 min at 4°C.

Anti-AGO2 (abcam), anti-AGO1 (N-terminal, Sigma), anti-HA (Sigma) and anti-TERT (C-12, Santacruz) antibodies as well as isotype-matched immunoglobulin were coupled to Protein G-sepharose beads in IP-buffer containing 1 mg/ml heparin (Sigma). Whole-cell lysate was incubated overnight at 4°C with antibodies-coupled beads. IP was washed once with IP-buffer and three times with IP-wash buffer (50 mM Tris-HCl, pH 7.5; 300 mM NaCl; 5 mM MgCl2; and 0.05% Nonidet P-40). An aliquot of IP was saved for western blot analysis. TriFast (0.6 ml) (Euroclone) was added to the rest of each IP sample.

RNA isolation and qRT-PCR

Total RNA as well as RIP samples were isolated using Direct-zol™ RNA MiniPrep Kit (Zymo Research) according to manufacturer's protocol. Reverse transcription was performed from 200 ng of total RNA or 1/10 of RIP samples, using GoScript™ Reverse Transcriptase (Promega), following manufacturer's protocol. Random primers (Promega) or oligo(dT)$_{15}$ were used for total RNA or polyadenylated RNA reverse transcription, respectively. qPCR was performed with GoTaq® qPCR Master Mix (Promega) and primers were as follows: TERC Fw GCGAAGAGTTGGGCTCTGTCA, Rev TTCCTCTTCCTGCGGCCTGAAA; 3' extended TERC Fw CTTTCAGGCCGCAGGAAGAGGAA, Rev GGTGACGGATGCGCACGAT; HPRT1 Fw CAAAGATGGTCAAGGTCGC, Rev TCAAATCCAACAAAGTCTGGC; HOTAIR Fw GGTAGAAAAAGCAACCACGAAGC, Rev ACATAAACCTCTGTCTGTGAGTGCC; 7SK Fw CCCCTGCTAGAACCTCCAAAC, Rev CACATGCAGCGCCTCATTT. EctoTERC was amplified by using a Fw primer mapping inside TERC coding sequence (AAGAGGAACGGAGCGAGTC) and a Rev primer mapping on the specific sequence at the 3'end of ectoTERC (GCATGTGTGAGCCGAGTC).

Target enrichment in IP sample was normalized using 7SK RNA enrichment, as an unrelated RNA [59], and calculated using the $2^{-\Delta\Delta Ct}$ method.

sRNA isolation and qRT-PCR

sRNA fraction (<100nt) was isolated by miRNA Isolation Kit (Genaid), accordingly to manufacturer's protocol. sRNA isolation was verified on a 2% agarose gel, where transfer-RNA was loaded as molecular weight reference. *terc*-sRNA expression was checked by using Custom TaqMan® Small RNA Assay (Thermo Fisher Scientific). One hundred ng of sRNAs or 1/10 of RIP samples was reverse transcribed using SuperScript II Reverse Transcriptase (Thermo Fisher Scientific) and qPCR was performed using iTaq Universal Probes Supermix (Biorad). Quantification was normalized to small nucleolar RNA U44, amplified by TaqMan® Small RNA Assay (Thermo Fisher Scientific).

Protein Isolation and Western blot

For whole-cell protein extracts, cells were lysed in RIPA Buffer (150mM NaCl, 1% NP-40, 0.5% Sodium deoxycholate, 0.1% SDS, 50mM Tris pH 8, 1mM DTT, protein inhibitor cocktail).

For Western blot analyses the following antibodies were used: anti-AGO2 (11A9, Millipore), anti-AGO1 (N-terminal, Sigma), anti-HA (F-7, Santacruz), anti-TERT (H-231, Santacruz), anti-GAPDH (14C10, Cell Signaling technology), GW182 (A302-329A, Bethyl Laboratories).

Microarray analysis

Total RNA from parental or AGO2KO HeLaS3 cells was isolated by TRI Reagent (Sigma), following manufacturer's protocol. Microarray was performed by The Genomics Core Facility (GeneCore) at EMBL (Heidelberg, Germany). GeneChip™ Human Gene 2.0 ST Array (Affymetrix) was used. Microarray data were analysed using R Bioconductor. Package "oligo" was used to import .cel files; library "hugene20sttranscriptcluster.db" was used for gene annotation; package "genefilter" was used for filtering; package "limma" was used for data analysis.

sRNA Seq analysis

Adapter sequences were removed using cutadapt[ref]. Reads were first aligned to human mirna hairpin sequences (mirBase 21). Unaligned reads were then aligned on human rRNA and tRNA database. Fianlly, all unaligned reads were aligned on hg38 human genome reference. All alignements were performed with bowtie1, using the following parameters: -n 2 -l 18. In the last alignement round only sequences with a single valid alignement were taken into account (option -m 1). Coverage plots were obtained using bedtools genomeCoverage.

RNA-hybrid analysis

Target sequences of *terc*-sRNA were identified using RNAhybrid 2.1.2 [27] using the option -s 3utr_human.

Data Avaibility

The datasets analyzed during the current study are available in the ENA repository (ERX350060, ERX338767, ERX344794, ERX344797), in the SRA repository (SRP022054, SRP028291, SRP014142, SRP045645, SRP003902, SRP048750) and in ArrayExpress (E-MTAB-7085).

REFERENCES

1. Weinrich SL, Pruzan R, Ma L, Ouellette M, Tesmer VM, Holt SE, Bodnar AG, Lichtsteiner S, Kim NW, Trager JB, et al. (1997) Reconstitution of human telomerase with the template RNA component hTR and the catalytic protein subunit hTRT. *Nat Genet* **17**: 498–502.

2. Egan ED, Collins K (2010) Specificity and Stoichiometry of Subunit Interactions in the Human Telomerase Holoenzyme Assembled In Vivo. *Mol Cell Biol* **30**: 2775–2786.

3. Wu RA, Upton HE, Vogan JM, Collins K (2017) Telomerase Mechanism of Telomere Synthesis. *Annu Rev Biochem* **86**: 439–460.

4. Armanios M, Blackburn EH (2012) The telomere syndromes. *Nat Rev Genet* **13**: 693–704.

5. Kim NW, Piatyszek MA, Prowse KR, Harley CB, West MD, Ho PL, Coviello GM, Wright WE, Weinrich SL, Shay JW (1994) Specific association of human telomerase activity with immortal cells and cancer. *Science* **266**: 2011–2015.

6. Shay JW, Bacchetti S (1997) A survey of telomerase activity in human cancer. *Eur J Cancer Oxf Engl 1990* **33**: 787–791.

7. Sasaki T, Shiohama A, Minoshima S, Shimizu N (2003) Identification of eight members of the Argonaute family in the human genome. *Genomics* **82**: 323–330.

8. Meister G, Landthaler M, Patkaniowska A, Dorsett Y, Teng G, Tuschl T (2004) Human Argonaute2 mediates RNA cleavage targeted by miRNAs and siRNAs. *Mol Cell* **15**: 185–197.

9. Carissimi C, Laudadio I, Cipolletta E, Gioiosa S, Mihailovich M, Bonaldi T, Macino G, Fulci V (2015) ARGONAUTE2 cooperates with SWI/SNF complex to determine nucleosome occupancy at human Transcription Start Sites. *Nucleic Acids Res* **43**: 1498–1512.

10. Zamudio JR, Kelly TJ, Sharp PA (2014) Argonaute-bound small RNAs from promoter-proximal RNA polymerase II. *Cell* **156**: 920–934.

11. Valen E, Preker P, Andersen PR, Zhao X, Chen Y, Ender C, Dueck A, Meister G, Sandelin A, Jensen TH (2011) Biogenic mechanisms and utilization of small RNAs derived from human protein-coding genes. *Nat Struct Mol Biol* **18**: 1075–1082.

12. Wei W, Ba Z, Gao M, Wu Y, Ma Y, Amiard S, White CI, Rendtlew Danielsen JM, Yang Y-G, Qi Y (2012) A role for small RNAs in DNA double-strand break repair. *Cell* **149**: 101–112.

13. Morris KV, Santoso S, Turner A-M, Pastori C, Hawkins PG (2008) Bidirectional transcription directs both transcriptional gene activation and suppression in human cells. *PLoS Genet* **4**: e1000258.

14. Janowski BA, Huffman KE, Schwartz JC, Ram R, Nordsell R, Shames DS, Minna JD, Corey DR (2006) Involvement of AGO1 and AGO2 in mammalian transcriptional silencing. *Nat Struct Mol Biol* **13**: 787–792.

15. Gao M, Wei W, Li M-M, Wu Y-S, Ba Z, Jin K-X, Li M-M, Liao Y-Q, Adhikari S, Chong Z, et al. (2014) Ago2 facilitates Rad51 recruitment and DNA double-strand break repair by homologous recombination. *Cell Res* **24**: 532–541.

16. Ameyar-Zazoua M, Rachez C, Souidi M, Robin P, Fritsch L, Young R, Morozova N, Fenouil R, Descostes N, Andrau J-C, et al. (2012) Argonaute proteins couple chromatin silencing to alternative splicing. *Nat Struct Mol Biol* **19**: 998–1004.

17. Tarallo R, Giurato G, Bruno G, Ravo M, Rizzo F, Salvati A, Ricciardi L, Marchese G, Cordella A, Rocco T, et al. (2017) The nuclear receptor ERβ engages AGO2 in regulation of gene transcription, RNA splicing and RISC loading. *Genome Biol* **18**: 189.

18. Laudadio I, Formichetti S, Gioiosa S, Klironomos F, Rajewsky N, Macino G, Carissimi C, Fulci V (2018) Characterization of Transcription Termination-Associated RNAs: New Insights into their Biogenesis, Tailing, and Expression in Primary Tumors. *Int J Genomics* **2018**:.

19. Eichhorn SW, Guo H, McGeary SE, Rodriguez-Mias RA, Shin C, Baek D, Hsu S, Ghoshal K, Villén J, Bartel DP (2014) mRNA Destabilization Is the Dominant Effect of Mammalian MicroRNAs by the Time Substantial Repression Ensues. *Mol Cell* **56**: 104–115.

20. Salone V, Rederstorff M (2015) Stem-loop RT-PCR based quantification of small non-coding RNAs. *Methods Mol Biol Clifton NJ* **1296**: 103–108.

21. Song G, Wang R, Guo J, Liu X, Wang F, Qi Y, Wan H, Liu M, Li X, Tang H (2015) miR-346 and miR-138 competitively regulate hTERT in GRSF1- and AGO2-dependent manners, respectively. *Sci Rep* **5**: 15793.

22. Westin ER, Chavez E, Lee KM, Gourronc FA, Riley S, Lansdorp PM, Goldman FD, Klingelhutz AJ (2007) Telomere restoration and extension of proliferative lifespan in dyskeratosis congenita fibroblasts. *Aging Cell* **6**: 383–394.

23. Cawthon RM (2002) Telomere measurement by quantitative PCR. *Nucleic Acids Res* **30**: e47.

24. Mender I, Shay JW (2015) Telomerase Repeated Amplification Protocol (TRAP). *Bio-Protoc* **5**:.

25. Moon DH, Segal M, Boyraz B, Guinan E, Hofmann I, Cahan P, Tai AK, Agarwal S (2015) Poly(A)-specific ribonuclease (PARN) mediates 3'-end maturation of the telomerase RNA component. *Nat Genet* **47**: 1482–1488.

26. Tseng C-K, Wang H-F, Burns AM, Schroeder MR, Gaspari M, Baumann P (2015) Human Telomerase RNA Processing and Quality Control. *Cell Rep* **13**: 2232–2243.

27. REHMSMEIER M, STEFFEN P, HÖCHSMANN M, GIEGERICH R (2004) Fast and effective prediction of microRNA/target duplexes. *RNA* **10**: 1507–1517.

28. Daugaard I, Hansen TB (2017) Biogenesis and Function of Ago-Associated RNAs. *Trends Genet TIG* **33**: 208–219.

29. Cummins JM, He Y, Leary RJ, Pagliarini R, Diaz LA, Sjoblom T, Barad O, Bentwich Z, Szafranska AE, Labourier E, et al. (2006) The colorectal microRNAome. *Proc Natl Acad Sci U S A* **103**: 3687–3692.

30. Wang D, Zhang Z, O'Loughlin E, Lee T, Houel S, O'Carroll D, Tarakhovsky A, Ahn NG, Yi R (2012) Quantitative functions of Argonaute proteins in mammalian development. *Genes Dev* **26**:

693–704.

31. Dueck A, Ziegler C, Eichner A, Berezikov E, Meister G (2012) microRNAs associated with the different human Argonaute proteins. *Nucleic Acids Res* **40**: 9850–9862.

32. Burroughs AM, Ando Y, de Hoon MJL, Tomaru Y, Suzuki H, Hayashizaki Y, Daub CO (2011) Deep-sequencing of human Argonaute-associated small RNAs provides insight into miRNA sorting and reveals Argonaute association with RNA fragments of diverse origin. *RNA Biol* **8**: 158–177.

33. Petri S, Dueck A, Lehmann G, Putz N, Rüdel S, Kremmer E, Meister G (2011) Increased siRNA duplex stability correlates with reduced off-target and elevated on-target effects. *RNA N Y N* **17**: 737–749.

34. Calin GA, Croce CM (2006) MicroRNA signatures in human cancers. *Nat Rev Cancer* **6**: 857–866.

35. Esteller M (2011) Non-coding RNAs in human disease. *Nat Rev Genet* **12**: 861–874.

36. Bertuch AA (2016) The molecular genetics of the telomere biology disorders. *RNA Biol* **13**: 696–706.

37. Ozturk MB, Li Y, Tergaonkar V (2017) Current Insights to Regulation and Role of Telomerase in Human Diseases. *Antioxid Basel Switz* **6**:.

38. Wang D, Zhang Z, O'Loughlin E, Lee T, Houel S, O'Carroll D, Tarakhovsky A, Ahn NG, Yi R (2012) Quantitative functions of Argonaute proteins in mammalian development. *Genes Dev* **26**: 693–704.

39. Mitchell JR, Wood E, Collins K (1999) A telomerase component is defective in the human disease dyskeratosis congenita. *Nature* **402**: 551–555.

40. Walne AJ, Vulliamy T, Marrone A, Beswick R, Kirwan M, Masunari Y, Al-Qurashi F, Aljurf M, Dokal I (2007) Genetic heterogeneity in autosomal recessive dyskeratosis congenita with one subtype due to mutations in the telomerase-associated protein NOP10. *Hum Mol Genet* **16**: 1619–1629.

41. Vulliamy T, Beswick R, Kirwan M, Marrone A, Digweed M, Walne A, Dokal I (2008) Mutations in the telomerase component NHP2 cause the premature ageing syndrome dyskeratosis congenita. *Proc Natl Acad Sci* **105**: 8073–8078.

42. Stanley SE, Gable DL, Wagner CL, Carlile TM, Hanumanthu VS, Podlevsky JD, Khalil SE, DeZern AE, Rojas-Duran MF, Applegate CD, et al. (2016) Loss-of-function mutations in the RNA biogenesis factor NAF1 predispose to pulmonary fibrosis–emphysema. *Sci Transl Med* **8**: 351ra107-351ra107.

43. Majumder M, House R, Palanisamy N, Qie S, Day TA, Neskey D, Diehl JA, Palanisamy V (2016) RNA-Binding Protein FXR1 Regulates p21 and TERC RNA to Bypass p53-Mediated Cellular Senescence in OSCC. *PLoS Genet* **12**: e1006306.

44. Robart AR, Collins K (2010) Investigation of human telomerase holoenzyme assembly,

activity, and processivity using disease-linked subunit variants. *J Biol Chem* **285**: 4375–4386.

45. Boyraz B, Bellomo CM, Fleming MD, Cutler CS, Agarwal S (2016) A novel TERC CR4/CR5 domain mutation causes telomere disease via decreased TERT binding. *Blood* **128**: 2089–2092.

46. Stone MD, Mihalusova M, O'Connor CM, Prathapam R, Collins K, Zhuang X (2007) Stepwise protein-mediated RNA folding directs assembly of telomerase ribonucleoprotein. *Nature* **446**: 458.

47. Kellermann G, Kaiser M, Dingli F, Lahuna O, Naud-Martin D, Mahuteau-Betzer F, Loew D, Ségal-Bendirdjian E, Teulade-Fichou M-P, Bombard S (2015) Identification of human telomerase assembly inhibitors enabled by a novel method to produce hTERT. *Nucleic Acids Res* **43**: e99.

48. O'Connor CM, Collins K (2006) A Novel RNA Binding Domain in Tetrahymena Telomerase p65 Initiates Hierarchical Assembly of Telomerase Holoenzyme. *Mol Cell Biol* **26**: 2029–2036.

49. Huang V, Li L-C (2014) Demystifying the nuclear function of Argonaute proteins. *RNA Biol* **11**: 18–24.

50. Wong JMY, Kyasa MJ, Hutchins L, Collins K (2004) Telomerase RNA deficiency in peripheral blood mononuclear cells in X-linked dyskeratosis congenita. *Hum Genet* **115**: 448–455.

51. Vulliamy T, Marrone A, Goldman F, Dearlove A, Bessler M, Mason PJ, Dokal I (2001) The RNA component of telomerase is mutated in autosomal dominant dyskeratosis congenita. *Nature* **413**: 432–435.

52. Sanjana NE, Shalem O, Zhang F (2014) Improved vectors and genome-wide libraries for CRISPR screening. *Nat Methods* **11**: 783–784.

53. Cawthon RM (2002) Telomere measurement by quantitative PCR. *Nucleic Acids Res* **30**: e47.

54. Wang F, Pan X, Kalmbach K, Seth-Smith ML, Ye X, Antumes DMF, Yin Y, Liu L, Keefe DL, Weissman SM (2013) Robust measurement of telomere length in single cells. *Proc Natl Acad Sci U S A* **110**: E1906-1912.

55. Berardinelli F, Antoccia A, Cherubini R, De Nadal V, Gerardi S, Cirrone G a. P, Tanzarella C, Sgura A (2010) Transient activation of the ALT pathway in human primary fibroblasts exposed to high-LET radiation. *Radiat Res* **174**: 539–549.

56. Perner S, Brüderlein S, Hasel C, Waibel I, Holdenried A, Ciloglu N, Chopurian H, Nielsen KV, Plesch A, Högel J, et al. (2003) Quantifying telomere lengths of human individual chromosome arms by centromere-calibrated fluorescence in situ hybridization and digital imaging. *Am J Pathol* **163**: 1751–1756.

57. Mender I, Shay JW (2015) Telomerase Repeated Amplification Protocol (TRAP). *Bio-Protoc* **5**:.

58. Campeau E, Ruhl VE, Rodier F, Smith CL, Rahmberg BL, Fuss JO, Campisi J, Yaswen P, Cooper PK, Kaufman PD (2009) A Versatile Viral System for Expression and Depletion of Proteins in Mammalian Cells. *PLOS ONE* **4**: e6529.

59. Chen X, He L, Zhao Y, Li Y, Zhang S, Sun K, So K, Chen F, Zhou L, Lu L, et al. (2017) *Malat1* regulates myogenic differentiation and muscle regeneration through modulating MyoD transcriptional activity. *Cell Discov* **3**: 17002.

Acknowledgments

We thank Dr. G. Meister for providing VP5- FLAG/HA AGO2 plasmid and Prof. Giuseppe Macino for scientific discussion. This work was supported by an EPIGEN (MIUR-CNR) grant to VF, by a grant MIUR Progetti Avvio alla Ricerca Sapienza Università di Roma to IL, and by a grant MIUR Progetti di Ateneo Sapienza Università di Roma to CC.

Author contributions: IL, CC and VF conceived and designed the study; IL, CC, DT, FO, GA, CC, FB, EC, AS carried out the experiments; VF and SG performed computational analysis; IL drafted the manuscript with input from all authors.

Conflicts of Interest

The authors declare that there is no conflict of interest regarding the publication of this article

Figure legends

Figure 1. AGO2 depletion in human cells reduces proliferation rate in *vitro* and tumor growth *in vivo*.

A. Proliferation curves of parental and AGO2KO HeLaS3 cells are plotted (n=6 experimental replicates).

B. Colony-forming activity of HeLaS3 and AGO2KO cells was determined by colony-formation assay (n=3 experimental replicates).

C. Tumour growth curves of xenografts derived from HeLaS3 or AGO2KO cells are shown as tumour diameter at different time points (n=5 mice for each group).

D. Xenograft tumour weights were measured 30 days post- injection (n=5 mice for each group).

Data information. Data are expressed as mean ± SEM. *P≤ 0.05; **P≤ 0.01; ***P≤ 0.01 (Student's t-test)

Figure 2. AGO2 interacts with a sRNA arising from TERC locus (*terc*-sRNA)

A. TERC RNA secondary structure (adapted from http://telomerase.asu.edu). *Terc*- sRNA is

highlighted in purple

B. HeLaS3 cells were transduced with a lentiviral vector coding for human *TERC* (HeLaS3_TERC) or for GFP, as a control (HeLaS3_GFP). The relative expression of TERC was measured by RT–qPCR. HPRT1 was used as internal control (n = 3 experimental replicates).

C. The relative expression of *terc*-sRNA was measured in HeLaS3_TERC and HeLaS3_GFP by RT–qPCR. RNU44 was used as internal control (n = 3 experimental replicates).

Data information. Data are expressed as mean ± SEM. *P≤ 0.05; ***P≤ 0.01 (Student's t-test).

Figure 3. AGO2 controls telomere length and telomerase activity.

A. Average telomere length was measured from genomic DNA of parental and AGO2KO HeLaS3, by qPCR amplification of telomere repeats (T) and multicopy gene Alu (R), as a reference. The relative telomere length (T/R) was plotted (n=3 experimental replicates)

B. Representative images of metaphase spreads obtained from HeLaS3 and AGO2KO cells stained for telomeric sequences and centromere 2 alphoid DNA.

C. Representative telomere length distributions in parental and AGO2KO HeLaS3. Average telomere length and the standard deviation, as well as the total number of telomeres analyzed, are indicated. Notice the marked shift towards short telomeres in AGO2KO cells compared with the parental HeLa S3 cell line.

D, E. Telomerase activity was detected by TRAP in parental HeLaS3 and AGO2KO cells. 293T cells were used as a positive control. As negative controls, telomerase was heat- inactivated in cell extracts, in the last lane no cells were added in lysis buffer. Intensity of the telomerase products (6 bp-ladder) was determined by ImageLab Software (Biorad) and normalized with the intensity of the Internal Control (IC) (n=3 experimental replicates).

F. AGO2KO cells were transduced with a lentiviral vector coding for FLAG-HA-tagged AGO2 (AGO2KO_FH AGO2) or for GFP as a control (AGO2KO_GFP). Quantification of telomerase activity in AGO2KO_FH AGO2 and AGO2KO_GFP, as assessed by TRAP, was plotted (n=3 experimental replicates).

G. HeLaS3 cells were transduced with a lentiviral vector coding for FLAG-HA-tagged AGO2 (HeLaS3_FH AGO2) or for GFP as a control (HeLaS3_GFP). Quantification of telomerase activity in HeLaS3_FH AGO2 and HeLaS3_GFP, as assessed by TRAP, was plotted (n=3 experimental replicates).

Data information. Data are expressed as mean ± SEM. *P≤ 0.05; **P≤ 0.01; ***P≤ 0.01 (Student's t-test)

Figure 4. AGO2 expression does not affect neither TERC RNA levels and 3'-end processing nor TERT protein abundance, but controls association between TERT and TERC.

A. The relative expression of TERC was measured by RT–qPCR from total RNA of HeLaS3 and AGO2KO cells. HPRT1 was used as internal control (n = 3 experimental replicates).

B. qPCR of 3'-extended TERC transcript in cDNA from HeLaS3 and AGO2KO cells generated using random hexamers. HPRT1 was used for normalization (n=3 experimental replicates).

C. qPCR of TERC transcript in cDNA from HeLaS3 and AGO2KO cells generated using oligo$(dT)_{10}$ priming. HPRT1 was used for normalization (n=3 experimental replicates).

D. Whole cell extract of HeLaS3 and AGO2KO was analyzed by western blot for the presence of TERT protein. GAPDH was used as loading control. Data are representative of 4 independent experiments.

E. TERT protein level was quantified by ImageLab Software (Biorad). GAPDH was use as internal control (n=4 experimental replicates)

F-G. HeLaS3 and AGO2KO cell extracts (n=3), as well as AGO2KO_FH AGO2 and AGO2KO_GFP cell extracts (n=3 experimental replicates) were immunoprecipitated using an anti-TERT antibody or IgG as mock IP. TERC and HOTAIR (as a negative control) abundance was assessed by RT-qPCR. HPRT1 was used for normalization and enrichment in TERT-RIP as compared to IgG RIP was plotted.

H. HeLaS3 whole-cell extract was immunoprecipitated using anti- AGO2 antibody or IgG, as mock IP. Whole cell lysates (input) and immunoprecipitates were analyzed by western blot with anti-TERT

antibody. As a positive control, the presence in immunoprecipitates of GW182, a known AGO2-interacting protein, was assessed. Data are representative of three independent experiments.

Data information. Data are expressed as mean ± SEM. *P≤ 0.05; ns= not significant (Student's t-test)

Figure 5. AGO2 is bound to TERC RNA and deletion of TERC regions complementary to *terc*-sRNA impairs AGO2/TERC interaction.

A. HeLaS3 whole-cell extract was immunoprecipitated using anti- AGO2 antibody or IgG, as mock IP. TERC RNA enrichment in AGO2 RIP as compared to IgG RIP was assessed by RT-qPCR . 7SK RNA was used for normalization (n=4 experimental replicates).

B. RIP assay was performed from HeLaS3_FH AGO2 and HeLaS3_GFP cell extract using anti-HA antibody or IgG, as negative control, followed by TERC detection by RT-qPCR. 7SK RNA was used for normalization (n=3 experimental replicates).

C. HeLaS3 cells were transduced with a lentiviral vector coding for wild-type TERC (HeLaS3_TERCwt), TERC mutated in position 313-340 (HeLaS3_TERC (313-340mut)) or TERC delated in position 12-31 (HeLaS3_TERC (Δ 12-31)). Whole-cell lysates from HeLaS3_TERCwt, HeLaS3_TERC(313-340mut) and HeLaS3_TERC (Δ 12-31) was immunoprecipitated using an anti-AGO2 antibody in order to assessed the impact of TERC mutations on AGO2 binding. For each experiment the enrichment of ectoTERC as compared to 7SK RNA in RIP samples was normalized on the amount of ectoTERC and 7SK RNA in input samples. Association of AGO2 with TERC(313-340mut and TERC (Δ 12-31) was compared to the association with TERCwt (n=3 experimental replicates).

Data information. Data are expressed as mean ± SEM. *P≤ 0.05; **P≤ 0.01; ***P≤ 0.01 (Student's t-test)

Figure 6. *Terc*-sRNA overexpression increases telomerase activity even in the absence of AGO2.

A-B. HeLaS3 and AGO2KO cells were transfected with a synthetic *terc*-sRNA or an siRNA with no target in humans (siCtl), as a control. Four days after transfection, telomerase activity in 100- and 50 cell-lysate was assessed by TRAP. Intensity of the telomerase products (6 bp-ladder) was determined

by ImageLab Software (Biorad) and normalized with the intensity of the Internal Control (IC), (n=4 experimental replicates)

Data information. Data are expressed as mean ± SEM. *P≤ 0.05; **P≤ 0.01 (Student's t-test)

Expanded View Figure Legend

Fig EV1. The newly identified AGO2-bound *terc*-sRNA is processed in a DICER- and AGO2-independent manner.

A. Coverage of a sRNA (23 nt) arising from positions 425 to 447 of mature TERC RNA (terc- sRNA), as assessed by sRNA-Seq of nuclear AGO2-IP from HCT116 and HeLaS3 cells.

B. Validation of sRNA-Seq was performed by immunoprecipitating AGO2-bound RNA from HeLaS3 whole-cell extract using a different anti-AGO2 antibody or IgG, as negative control. Immunoprecipitation was verified by western blot.

C. RIP assay was performed from HeLaS3 whole-cell extract using anti- AGO2 antibody or IgG, as negative control. *Terc*-sRNA enrichment in AGO2 RIP as compared to IgG RIP was assessed by RT-qPCR. 7SK RNA was used for normalization (n=3 experimental replicates).

D-G. *Terc*-sRNA, miR-21, miR-30a and let7f abundance was assessed in small RNA (< 100nt) fractions of HCT116 and HCT116 DICER^{EX5} (D, E) and of HeLaS3 and AGO2KO cells (F, G). RNU44 was used as internal control (n = 3 experimental replicates).

Data information. Data are expressed as mean ± SEM. *P≤ 0.05; ns= not significant (Student's t-test).

Fig EV2. AGO1 binds to *terc*-sRNA and to TERC but AGO1 depletion does not affect telomerase activity neither in wild type nor in AGO2KO background.

A. Coverage of terc-sRNA, as assessed by sRNA-Seq of nuclear AGO1-IP from HeLaS3 cells.

B. RIP assay was performed from HeLaS3 cell extract using anti- AGO1 antibody or IgG, as negative control. Immunoprecipitation was verified by western blot.

C-D. TERC RNA (n=3 experimental replicates) and *terc*-sRNA (n=5 experimental replicates) enrichment in AGO1 RIP as compared to IgG RIP was assessed by RT-qPCR. 7SK RNA was used for normalization.

E. Telomerase activity was detected by TRAP in two HeLaS3 clones isolated following transduction with LentiCRISPR v2 control vector (HeLaS3 WT CRISP neg), in AGO2KO cells following transduction with LentiCRISPR v2 (AGO2KO CRISPR neg), two AGO1/AGO2 double KO clones isolated from AGO2KO cells following transduction with LentiAGO1CRISPR v2 (AGO1/AGO2dKO) and two AGO1 KO clones isolated from HeLaS3 cells following transduction with LentiAGO1CRISPR v2 (AGO1KO). Quantitative analysis of telomerase activity was plotted (n=3 experimental replicates).

Data information. Data are expressed as mean ± SEM. *P≤ 0.05; **P≤ 0.01; ns= not significant (Student's t-test).

Fig EV3. *Terc*-sRNA is expressed in human primary samples and over-expressed in cancerous tissues compared to control tissues

A. Coverage of terc-sRNA as assessed by sRNA-Seq from different primary tissues.

B. *Terc*-sRNA expression (RPM) in different tumor types compared to control tissues. Tumor datasets of sRNA-Seq are from SRA repository: SRP028291, SRP014142, SRP048750, SRP045645 and SRP003902, SRP022054 (Wilcoxon sum-rank test).

Laudadio_Fig 1

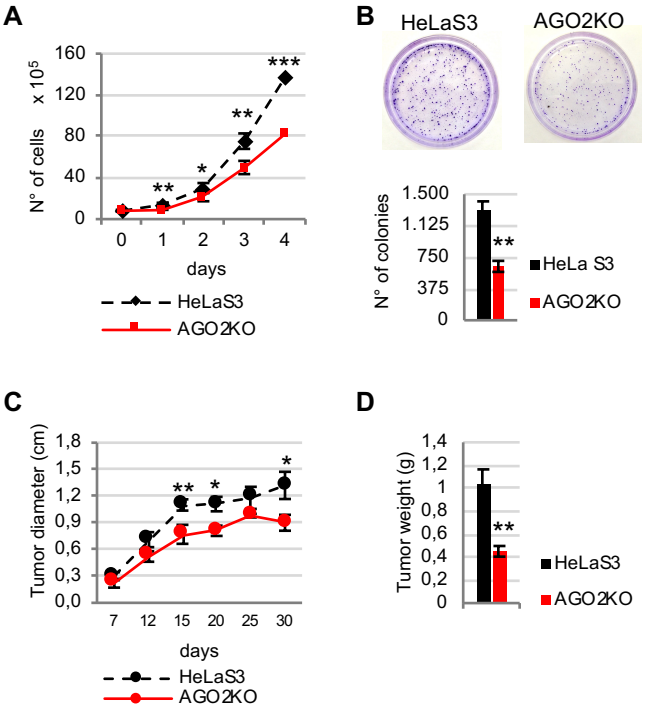

Laudadio_Fig2

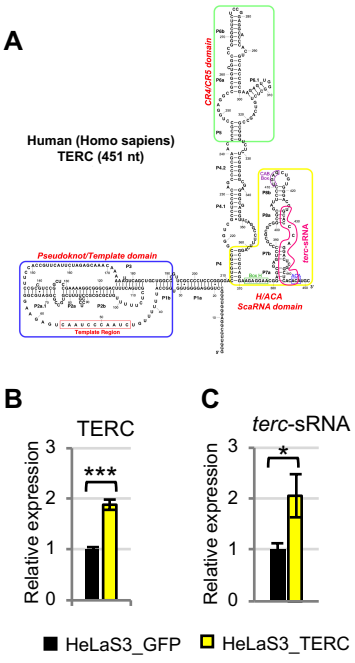

Laudadio_Fig3

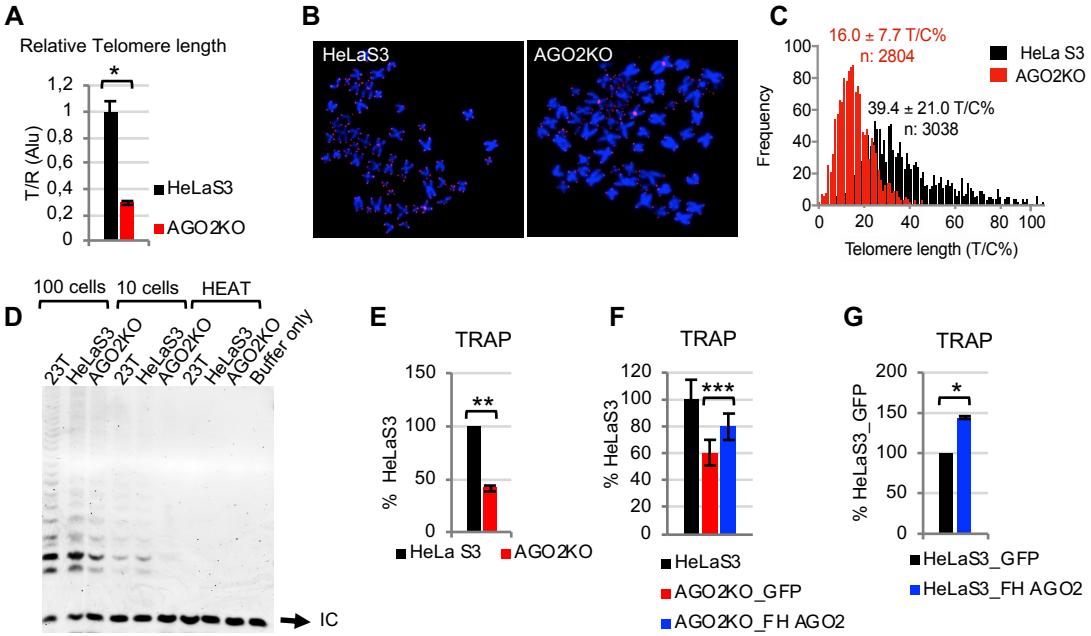

Laudadio_Fig4

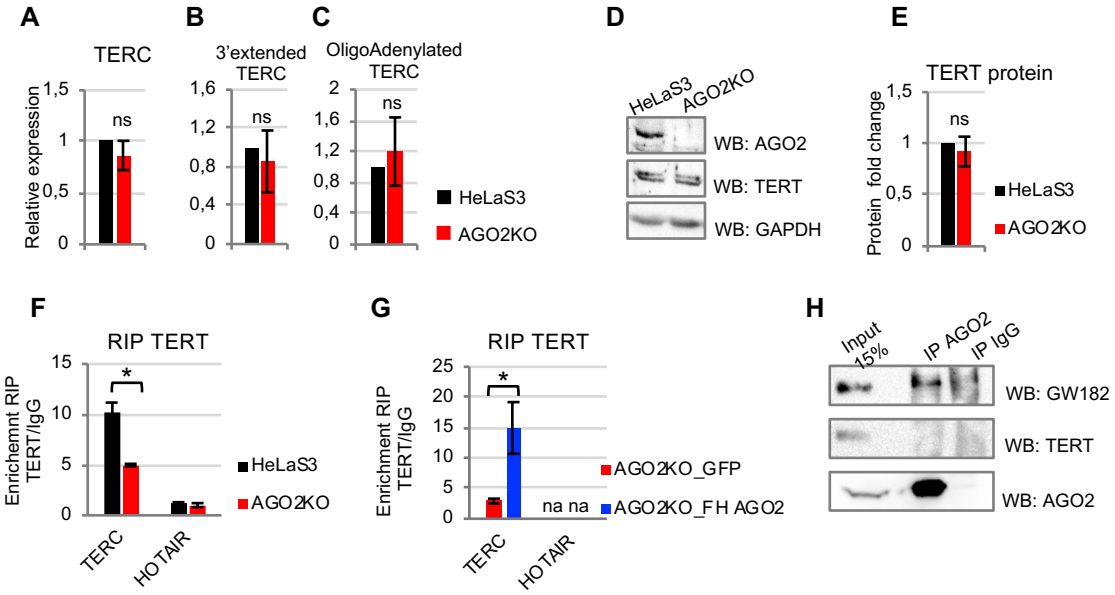

Laudadio_Fig5

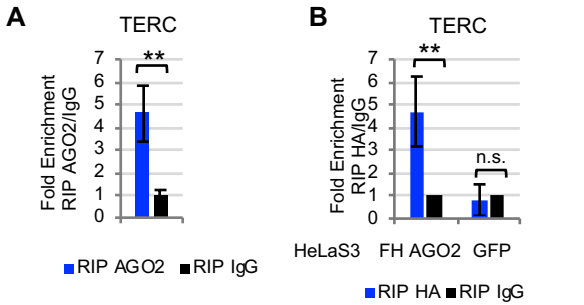

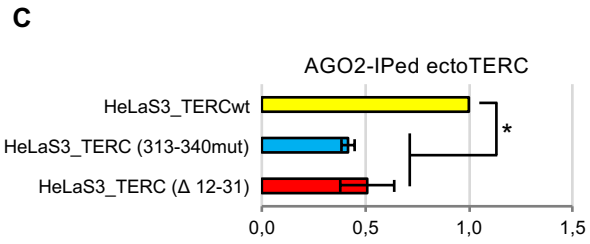

Laudadio_Fig6

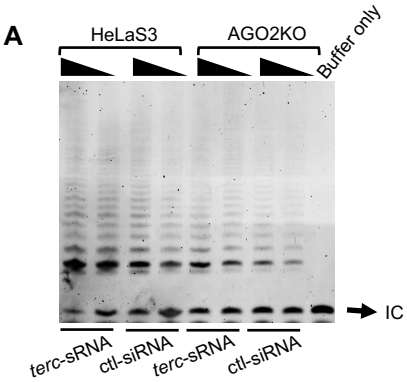

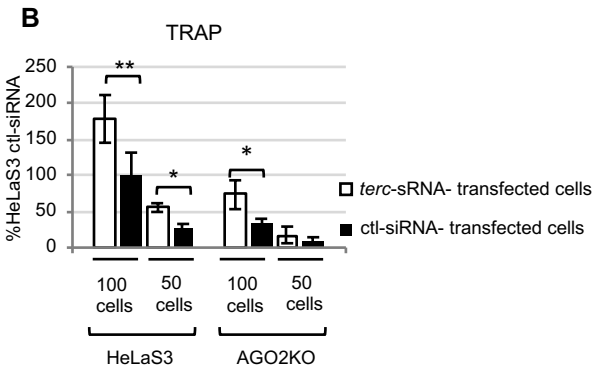

Laudadio_Fig EV1

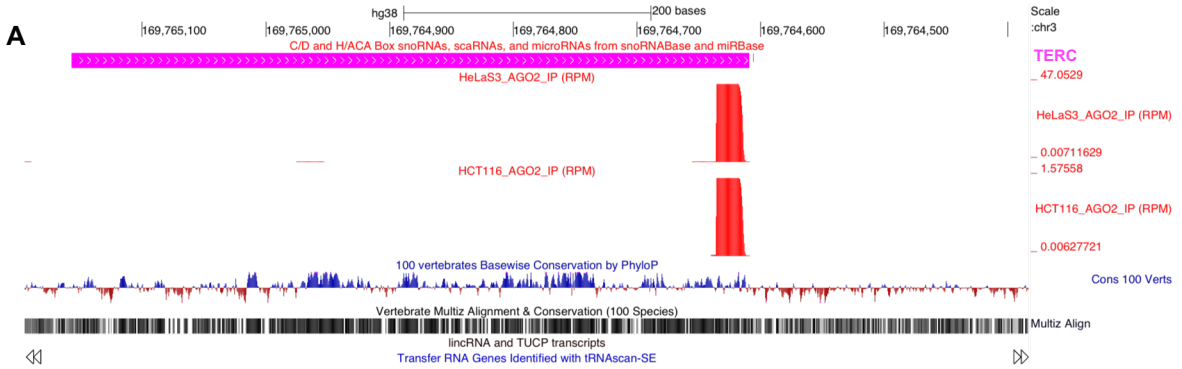

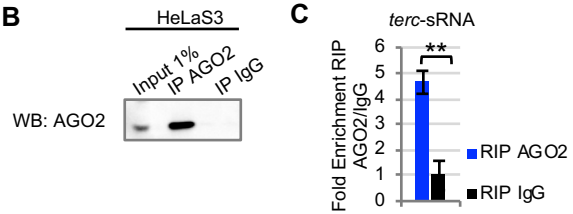

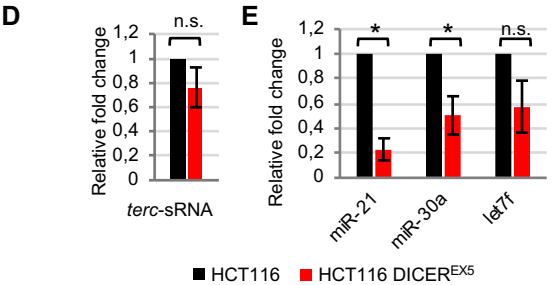

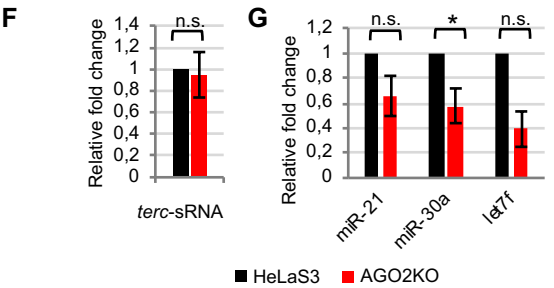

Laudadio_Fig EV2

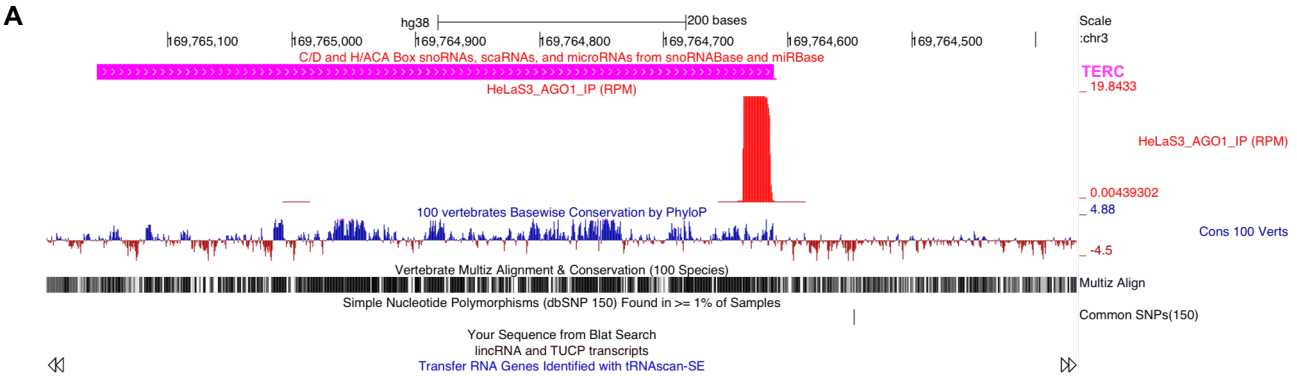

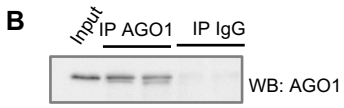

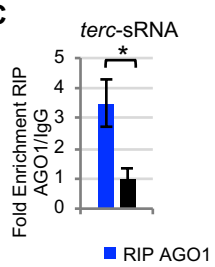

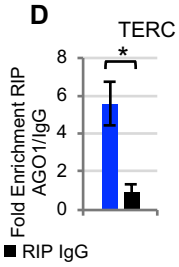

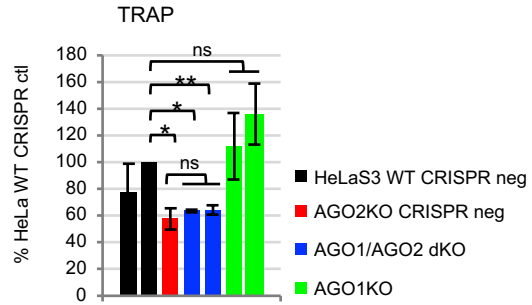

Laudadio_Fig EV3

A

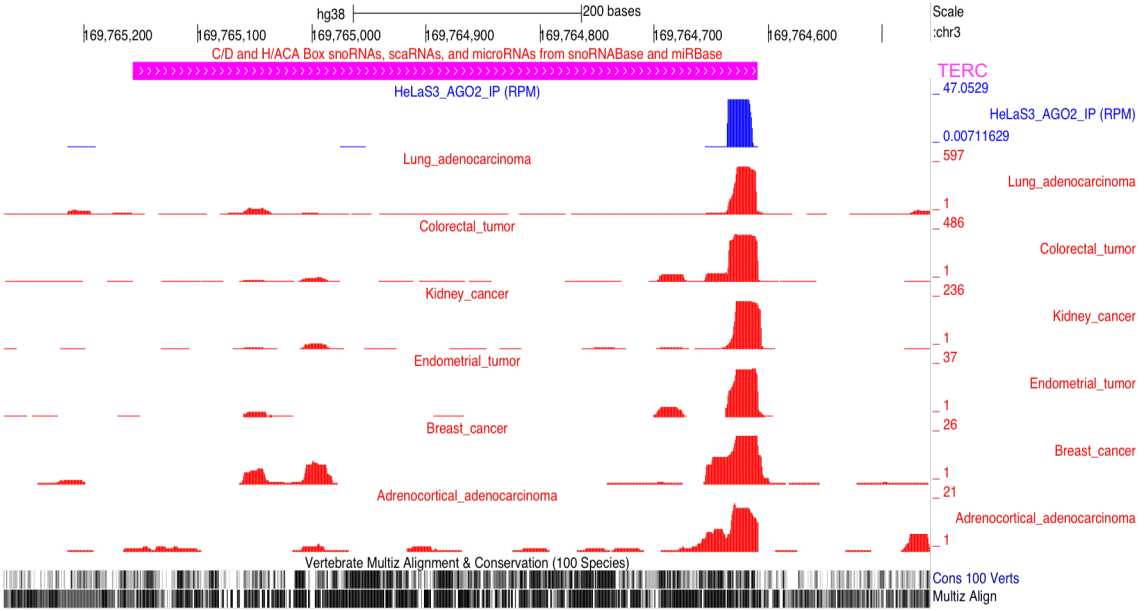

B

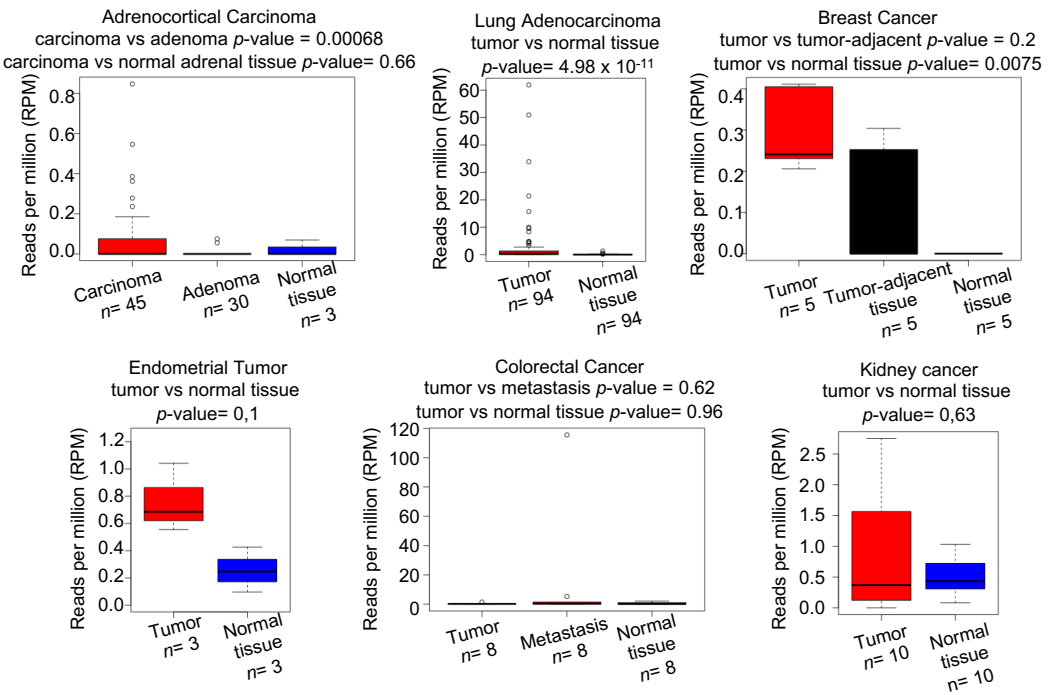

Appendix Files

Table of content

Appendix figure S1

A

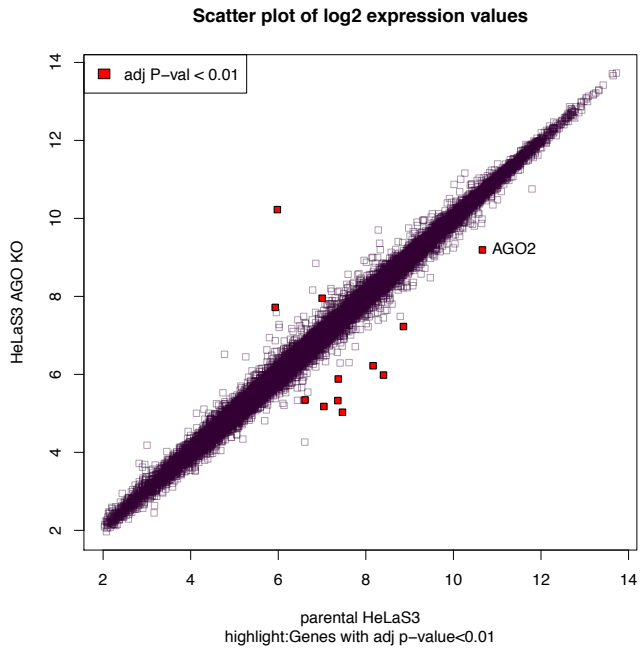

B

Gene Symbol	Gene Name	Linear fold change (AGO2KO/HeLaS3)*
RASEF	RAS and EF-hand domain containing	018
LINC00958	long intergenic non-protein coding RNA 958	0.19
ATRN	attractin	0.24
ALKBH3	alkB homolog 3, alpha-ketoglutaratedependent dioxygenase	0.26
TMPRSS15	transmembrane protease, serine 15	0.27
CDH13	cadherin 13	0.32
CACHD1	cache domain containing 1	0.36
AGO2	argonaute 2, RISC catalytic component	0.36
BICC1	BicC family RNA binding protein 1	0.42
SLCO1C1	solute carrier organic anion transporter family member 1C1	1.93
SORBS2	sorbin and SH3 domain containing 2	3.45
SRGN	serglycin	18.96

*FDR < 0.01

Appendix figure S1. A. Data from microarray are graphed on a scatter plot to visualize variations in gene expression between parental and AGO2KO HeLaS3 cells. Genes attaining statistical significance (FDR < 0.01) are highlighted in red. B. List of genes differentially expressed in AGO2KO cells as compared to parental cells, as assessed by microarray.

Appendix figure S2

A

	Sequence 5'>3'
***terc*-sRNA**	UGCACCCAGGACUCGGCUCACA

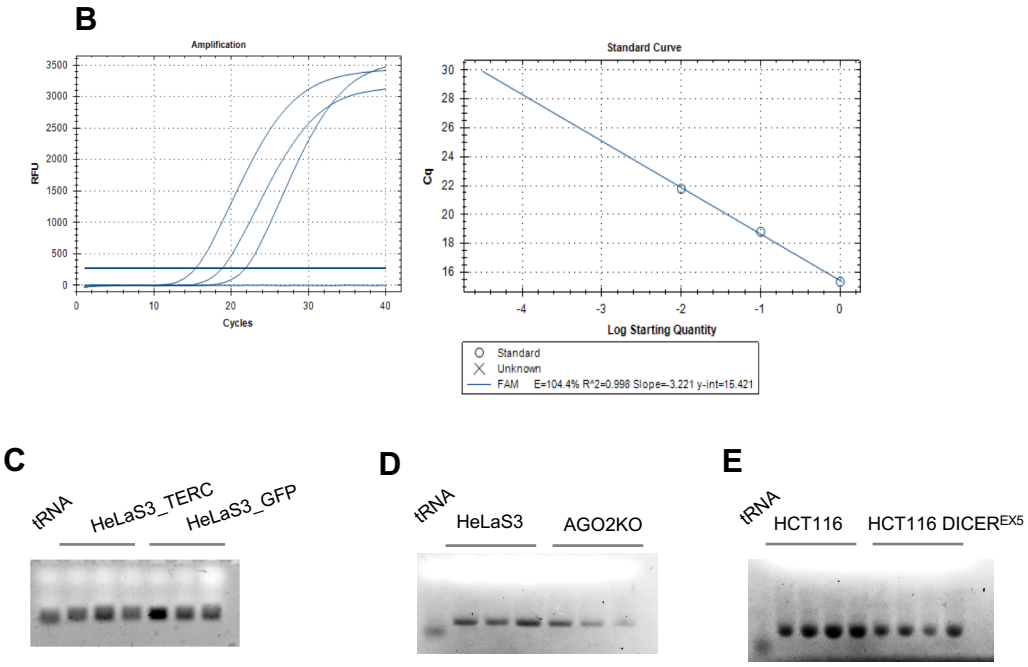

Appendix figure S2. A. *Terc*-sRNA sequence. B. *Terc*-sRNA was detected by qRT-PCR by a Custom TaqMan Small RNA Assay (cat. 4398987, Applied biosystems). One fmol of a synthetic double stranded *terc*-sRNA was reverse transcribed and qPCR primer efficiency was verified by amplification of 3 ten-fold serial dilutions of the reverse transcription reaction. C, D, E. Small RNA fraction (< 100 nt) was isolated from HeLaS3_TERC, HeLaS3_GFP, HeLaS3, AGO2KO, HCT116 and HCT116$^{DICER\ EX5}$. Transfer-RNA (tRNA) was loaded as molecular weight reference.

Appendix figure S3

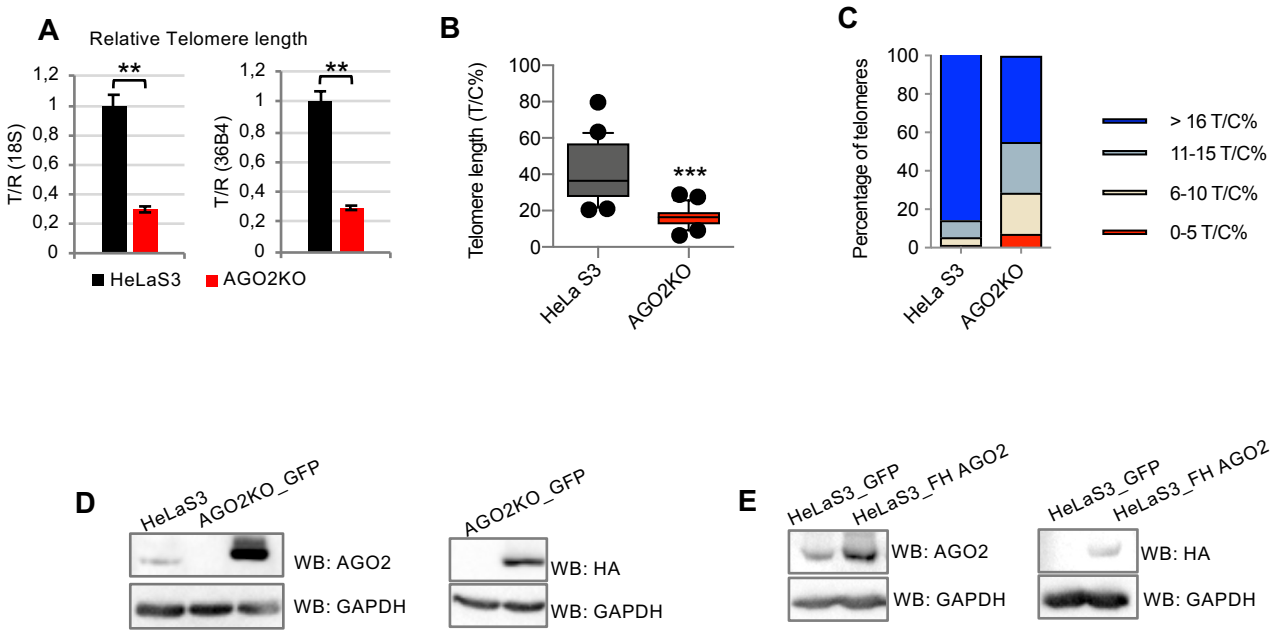

Appendix figure S3. A. Average telomere length was measured from genomic DNA of parental and AGO2KO HeLaS3, by qPCR amplification of telomere repeats (T) and the multicopy gene 18S or the four-copy gene 36B4 (R), as references. The relative telomere length (T/R) was plotted (n=3 experimental replicates). Data are expressed as mean ± SEM. **P≤ 0.01; (Student's t-test). B. Telomere length per metaphase in HeLa S3 and AGO2KO cell lines. Box plot represent median, 25th and 75th percentile whereas skewers represent 10th and 90th percentile. Black circles denote outliers (over 90th percentile and under 10th percentile) (n=22). ***P≤ 0.001; (Student's t-test). C. Stacked histograms showing percent of telomeres shorter than 5, 10 and 15 T/C% and longer than 16 T/C% in parental and AGO2KO HeLaS3 (n=2 experimental replicates). D, E. AGO2KO and HeLaS3 cells were transduced with a lentiviral vector coding for FLAG-HA-tagged AGO2 (AGO2KO_FH AGO2 and HeLaS3_FH AGO2, respectively) or for GFP as a control (AGO2KO_GFP and HeLaS3_GFP, respectively). Expression of ectopic protein was verified by western blot using anti-HA and anti-AGO2 antibodies. GAPDH was used as loading control

Appendix figure S4

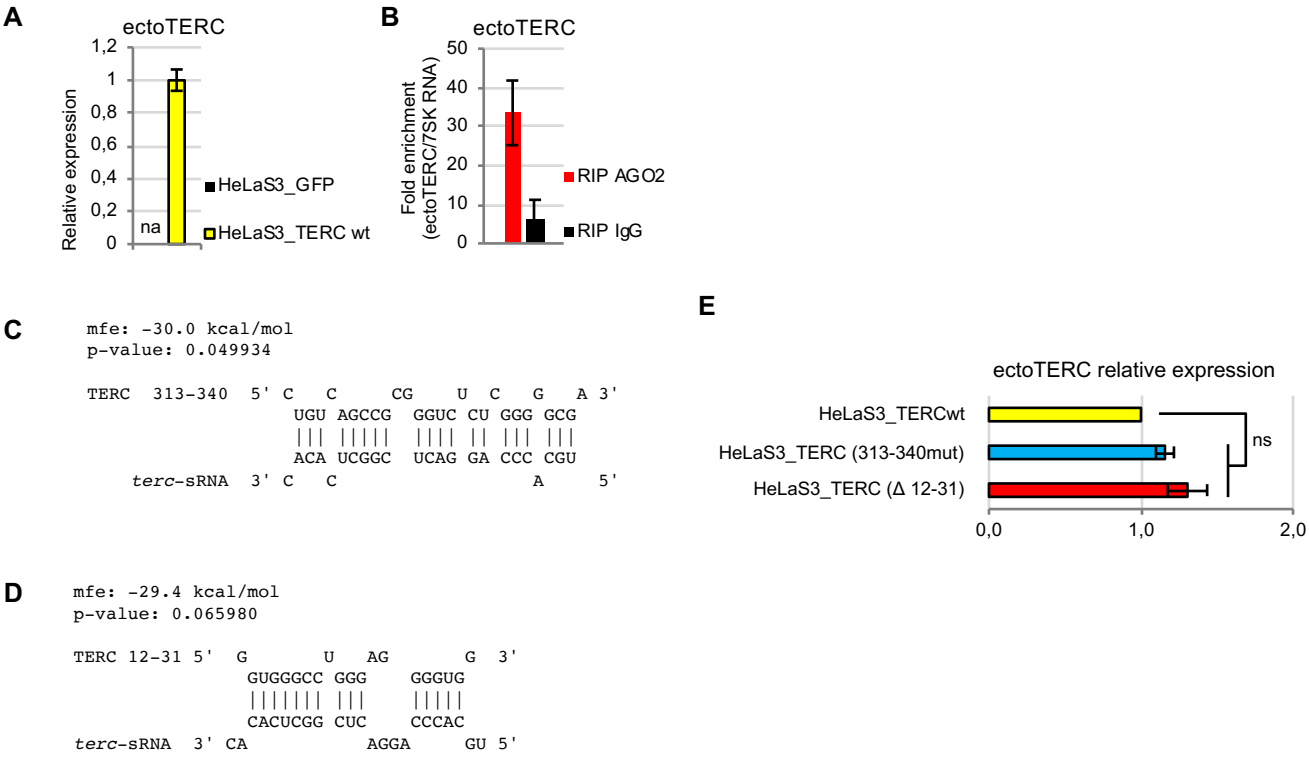

Appendix figure S4. A. HeLaS3 cells were transduced with a lentiviral vector coding for human TERC (HeLaS3_TERCwt) or for GFP, as a control (HeLaS3_GFP). The relative abundance of ectopically expressed TERC RNA (ectoTERC) was measured by RT–qPCR using primers which do not amplify endogenous TERC. HPRT1 was used as internal control (n=3 experimental replicates). B. RIP assay was performed from HeLaS3_TERCwt whole-cell extract using anti- AGO2 antibody or IgG, as negative control. EctoTERC enrichment in AGO2- and IgG RIP was assessed by RT-qPCR . 7SK RNA was used for normalization (n=3 experimental replicates). C-D. RNAhybrid prediction of the best minimum free energy (mfe) duplexes of *terc*-sRNA and TERC. E. The relative expression of ectoTERC was measured by RT–qPCR from total RNA of HeLaS3_TERCwt, HeLaS3_TERC (313-340mut) and HeLaS3_TERC (Δ 12-31) cells. 7SK RNA was used as internal control (n=3 experimental replicates).

Appendix figure S5

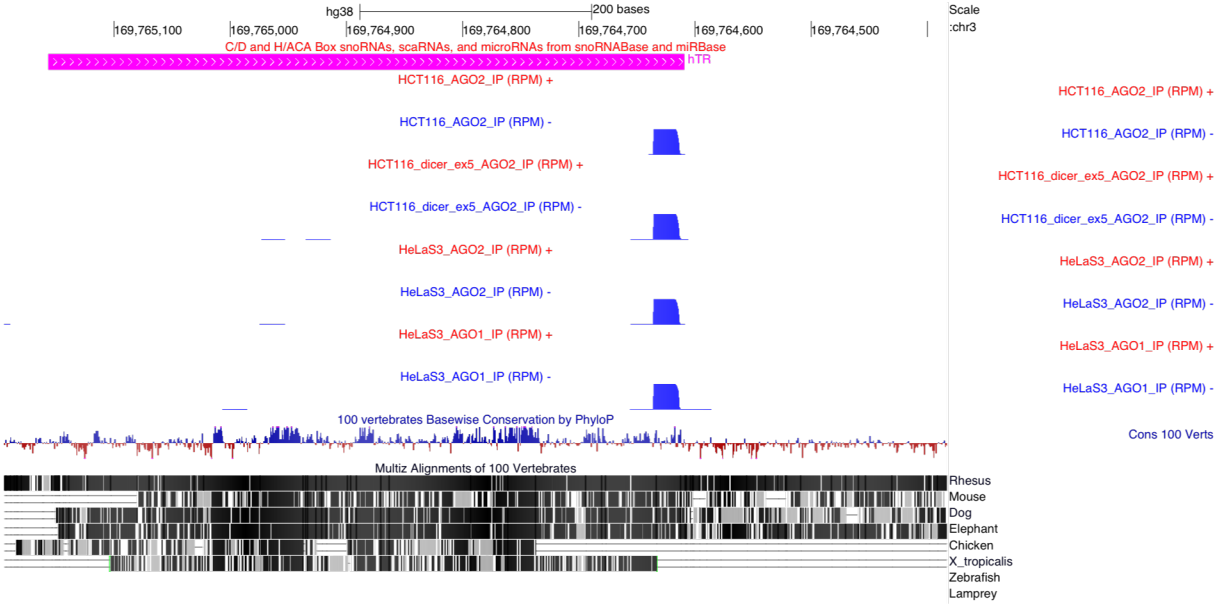

Appendix figure S5. Coverage of sRNA mapping on TERC gene from nuclear AGO2-RIP experiment in HCT116, HCT116 (DICER EX5), and HelaS3 and from nuclear AGO1-RIP in HelaS3. TERC RNA is transcribed from the - strand of DNA. Reads mapping to the - strand (sense orientation with respect to TERC transcription) are plotted in blue, whereas reads mapping to the + strand (anti-sense orientation with respect to TERC transcription) are plotted in red.

Appendix figure S6

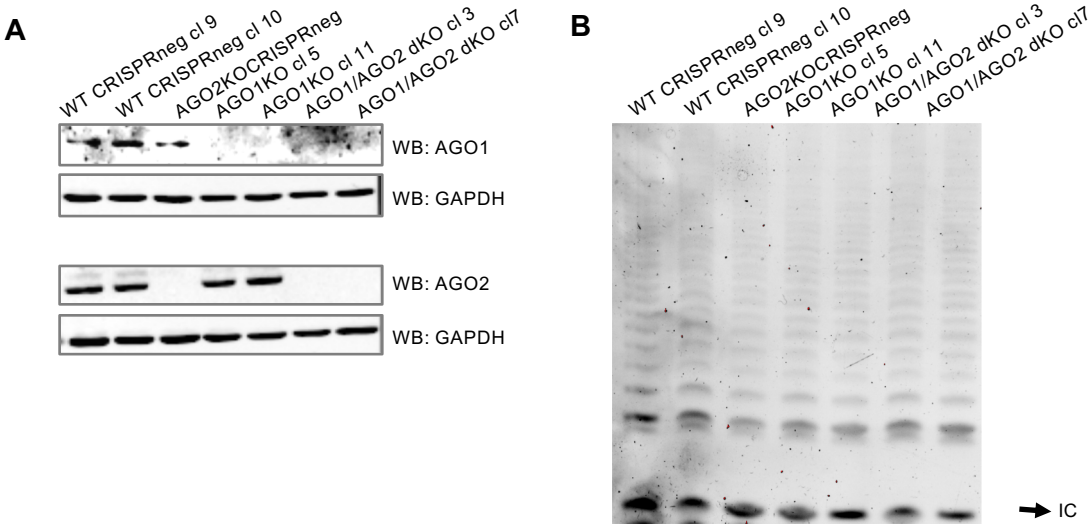

Appendix figure S6. A. CRISPR/Cas9 technology was used to generate AGO1KO and AGO1/AGO2dKO cell lines. Expression of AGO1 and AGO2 was verified by western blot in two HeLaS3 clones isolated following transduction with CRISPR/Cas9 control lentiviral vector (HeLaS3 WT CRISPR neg cl9 and cl10), in AGO2KO cells following transduction with CRISPR/Cas9 control vector (AGO2KO CRISPR neg), in two AGO1 KO clones isolated from HeLaS3 cells following transduction with AGO1-targeting CRISPR/Cas9 vector (AGO1KO cl5 and cl11) and in two AGO1/AGO2 double KO clones isolated from AGO2KO cells following transduction with AGO1-targeting CRISPR/Cas9 vector (AGO1/AGO2dKO cl3 and cl7). GAPDH was used as loading control. B. Telomerase activity was detected by TRAP in the indicated cell lines. Data are representative of three independent experiments. IC= internal control